Implications of eddy cancellation on nutrient distribution within subtropical gyres

Edward W. Doddridge[1,2], **David P. Marshall**[2]

[1]Earth, Atmospheric and Planetary Science, Massachusetts Institute of Technology, Cambridge, Massachusetts, USA
[2]Department of Physics, University of Oxford, Oxford, United Kingdom

Key Points:

- The impact of eddy cancellation on nutrients in oligotrophic gyres is studied in an idealized 2-layer model
- Modeled nutrient concentration responds non-monotonically to Ekman pumping and mode water thickness
- Mode water thickness is positively correlated with productivity in the Bermuda Atlantic Time-Series

Corresponding author: Edward W. Doddridge, ewd@mit.edu

Abstract

The role of mesoscale eddies within the nutrient budget of subtropical gyres remains poorly understood and poorly constrained. We explore a new mechanism by which mesoscale eddies may contribute to these nutrient budgets, namely eddy cancellation. Eddy cancellation describes the rectified effect of mesoscale eddies acting to oppose the Eulerian-mean Ekman pumping. We present an idealized axisymmetric two-layer model of a nutrient in a wind-driven gyre and explore the sensitivity of this model to variations in its parameter values. We find that the residual Ekman pumping velocity has a substantial impact on nutrient concentration, as does mode water thickness. These results suggest the response to both residual Ekman pumping and mode water thickness is non-monotonic: for small values of these parameters the nutrient concentration decreases as the parameter increases. However, beyond a critical value, further increases in Ekman pumping or mode water thickness increase nutrient concentration throughout our highly idealized model. A thin mode water layer promotes vertical diffusion of nutrients from the abyss, while a thicker mode water layer increases productivity by reducing the parametrized particulate flux through the thermocline. The impact of mode water thickness is modulated by the residual Ekman pumping velocity: strong Ekman pumping suppresses the influence of mode water thickness on nutrient concentrations. We use satellite and *in-situ* measurements to assess the influence of mode water thickness on primary productivity, and find a statistically significant relationship; thicker mode water correlates with higher productivity. This result is consistent with a small residual Ekman pumping velocity.

1 Introduction

The level of biological productivity varies dramatically across the ocean [*McClain et al.*, 2004]. The surface of the subtropical ocean is dominated by large regions of low nutrient concentration and low productivity. These areas of low nutrient concentration are referred to as oligotrophic. Despite the low productivity in these oligotrophic regions they contribute substantially to globally integrated marine production because they cover a large fraction of the ocean [*Jenkins and Doney*, 2003].

The nutrient budget of the oligotrophic ocean has been an area of active research for several decades. *Jenkins* [1982] used observations of tritium and helium to infer oxygen utilization rates. Their results suggested substantially larger downward fluxes of carbon from the upper sunlit region of the ocean, the euphotic zone, than had previously been assumed, and thus also a larger nutrient demand. There have since been many studies analyzing nutrient supply and productivity in the oligotrophic oceans in general, and the Sargasso Sea in particular [see, e.g., *Lee and Williams*, 2000; *Lévy*, 2008; *Lévy et al.*, 2012; *Martin and Pondaven*, 2003; *McClain et al.*, 2004; *McGillicuddy and Robinson*, 1997; *McGillicuddy et al.*, 1998, 2003; *Oschlies*, 2002a; *Pelegrí et al.*, 2006; *Williams and Follows*, 1998; *Williams et al.*, 2006]. Despite these efforts, there remain large uncertainties in the nutrient budget of the oligotrophic ocean. In particular, the role of mesoscale eddies in the nutrient budget of the euphotic zone is poorly constrained.

McGillicuddy and Robinson [1997] suggest that mesoscale eddies may be the dominant mechanism supplying nutrients to the euphotic zone of the oligotrophic ocean, delivering 0.35±0.10 mol nitrogen m^{-2} $year^{-1}$ through a mechanism they name "eddy pumping". Eddy pumping produces a vertical flux of nutrients into the euphotic zone by lifting nutrient rich water upwards into the euphotic zone through eddy-induced isopycnal heaving. This water is eventually pushed downwards out of the euphotic zone, but not before the nutrients are consumed by phytoplankton. However, *McGillicuddy and Robinson* [1997] use a simplified biogeochemical model that relaxes nutrient concentrations to climatological values below the euphotic zone, so their result represents an upper bound on the nutrient flux from eddy pumping. As eddies lift a fluid parcel into the euphotic zone the nutrients contained within that parcel are consumed and there is a flux of partic-

ulate matter downwards. This represents a diapycnal flux of nutrients downwards through the water column. *Oschlies* [2002b] notes that for eddy pumping to produce a steady state flux of nutrients into the euphotic zone, there needs to be a process that counteracts this downward flux and moves nutrients upwards towards the euphotic zone. *Jenkins and Doney* [2003] propose the "subtropical nutrient spiral", as a solution to this problem. As fluid circulates around a subtropical gyre, nutrients within the water are consumed and subsequently remineralised deeper within the fluid column. As the fluid containing the remineralised nutrients is advected into the western boundary current enhanced diapycnal diffusion moves the nutrients upwards towards the surface and they are returned to the euphotic zone in the gyre. However, this nutrient spiral is contradicted by the potential vorticity budget of *Polton and Marshall* [2007]. The nutrient spiral is also contradicted by *Burkholder and Lozier* [2014] who find that Lagrangian particles move deeper in the water column as they circulate around the North Atlantic subtropical gyre, rather than moving upwards in the western boundary current.

If the vertical transfer of nutrients by eddies is larger than the replenishment of nutrients at depth, then the effectiveness of eddy pumping will diminish with time. This effect is shown by *Lévy et al.* [2012] who run two versions of their model at different horizontal resolutions: one is a mesoscale resolving simulation at 1/9th of a degree; the other is a submesoscale permitting simulation at 1/54th of a degree. In the submesoscale permitting simulation the eddy activity is more vigorous, but after a transient peak the gyre averaged productivity is lower. This is due to the depletion of nutrients at depth, which reduces the efficiency of vertical eddy transfers. *Martin and Pondaven* [2003] compute the efficiency of eddy pumping in the subtropical North Atlantic and conclude that it is approximately 40 %, implying that previous altimetry based estimates of the eddy contribution to the nutrient budget, such as *Siegel et al.* [1999], had substantially overestimated the nutrient supply from eddy pumping.

Large-scale downwelling due to the convergence of Ekman transports in the subtropical gyres is often invoked as an explanation for the low productivity in these regions [see e.g. *Letscher et al.*, 2016; *Oschlies*, 2002a; *Williams and Follows*, 2011]. However, it has recently been suggested that the rectified effect of eddies opposes this Eulerian-mean Ekman pumping and effectively isolates the fluid above the thermocline from the nutrient rich abyss through a process called "eddy cancellation" [*Doddridge et al.*, 2016]. The key result from *Doddridge et al.* [2016] can be seen in figure 1 and in the animation included in the supplemental information. Using the Eulerian-mean velocities, which are obtained by taking the temporal average at each location, to advect particles in the subtropical gyre *Doddridge et al.* find that the particles move downwards through the thermocline. However, when mesoscale eddies are included by using the time-varying velocity fields, the particles remain above the thermocline. This suggests that mesoscale eddies are able to cancel the downwards motion due to Ekman pumping. It is important to recognize that eddy cancellation changes the diagnosed nutrient flux through an alteration of the background advective flow and is therefore distinct from the eddy pumping mechanism of [*McGillicuddy et al.*, 2003], which represents a direct nutrient flux. Here we investigate the implications of eddy cancellation for nutrient supply in subtropical gyres.

The remainder of this paper is structured as follows. In section 2 we introduce our idealized model and derive four coupled ordinary differential equations for nutrient concentration in oligotrophic gyres. In sections 2.1 and 2.2 we present solutions to these equations using the default parameter values, and investigate the nutrient budget of this model. In section 2.3 we test the sensitivity of our idealized model to variations in the parameter values. Section 3 tests the predicted sensitivity of productivity to mode water thickness using satellite and *in-situ* data. In section 4 we discuss some limitations of the idealized model and the observational analysis. In Section 5 we present our concluding remarks.

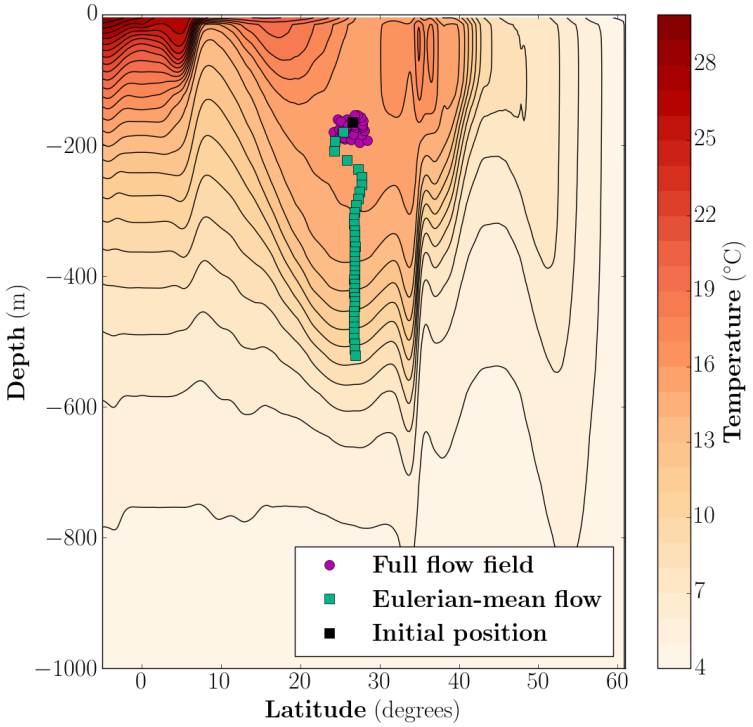

Figure 1. Results from a particle tracking experiment performed by *Doddridge et al.* [2016]. The purple circles show the centroid of approximately 6,000 particles tracked in the full velocity fields, while the green squares show the centroid of the particles tracked in the Eulerian-mean velocities, with three months of model time between subsequent markers; every three months each species of particle is reseeded in an ellipsoidal cloud around its center-of-mass. This reinitialization is discussed in more detail in *Doddridge et al.* [2016]. Ekman pumping is present in the Eulerian-mean velocity field, but not the full velocity field. The background colors represent a meridional slice of the time-averaged temperature field. An animation of the Lagrangian particle tracking experiment can be found in the supplementary information

2 1D model

Observational estimates of chlorophyll and productivity in the subtropical ocean both exhibit concentric regions with progressively lower values towards the center of the subtropical gyres, as seen in the satellite retrievals of chlorophyll concentration [*NASA Ocean Biology Processing Group*, 2015] in figure 2.

We seek to model the nutrient distribution in subtropical gyres with an idealized one-dimensional model. The model solves for the radial profile of phosphate concentration within a subtropical gyre. Our model consists of two active layers: a euphotic zone, and below that a mode water layer. Below the mode water layer is a nutrient rich, but quiescent abyss; any nutrients that are transported downwards through the thermocline at the base of the mode water layer are considered to be lost from the model. It should be noted that characterizing the dimensionality of our idealized model is not entirely straightforward. In the vertical, it is a box model with two active boxes and a lower boundary condition. However, in the horizontal our model retains one spatial dimension in its entirety, namely distance from the center of the gyre. Because it retains this spatial dimension in its entirety, we refer to our model as a one-dimensional model.

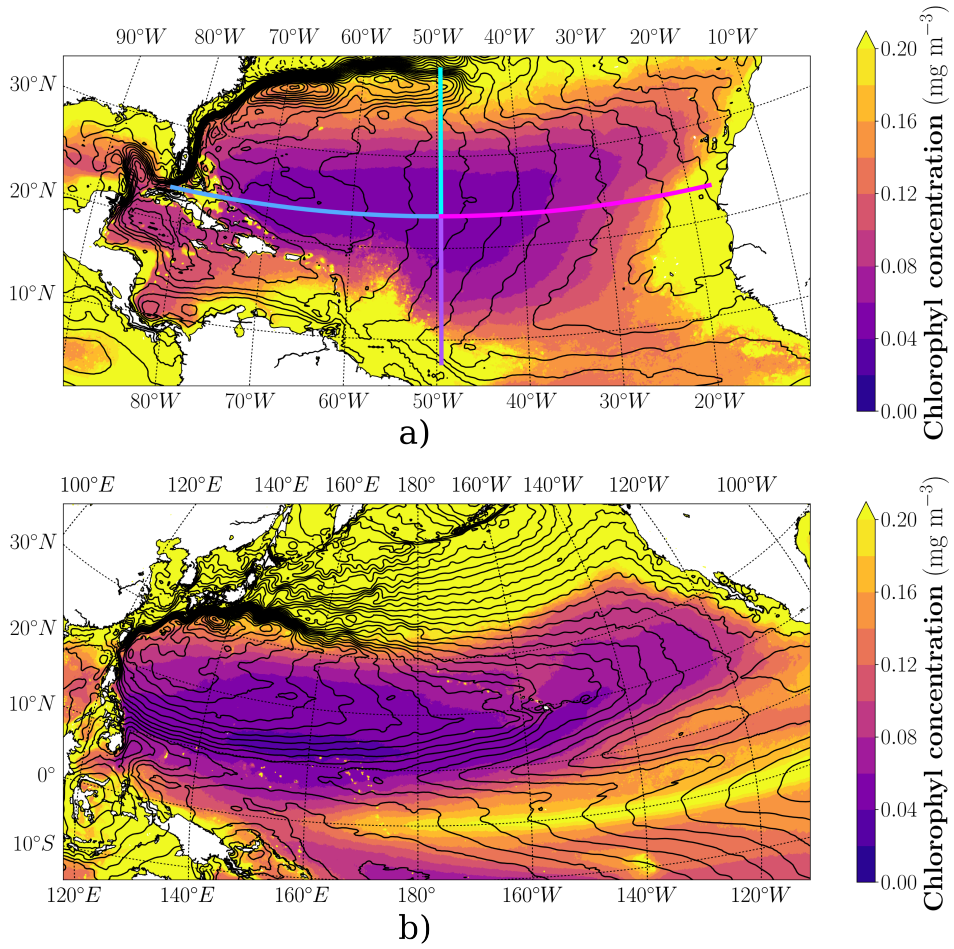

Figure 2. Mean chlorophyll concentration in **a)** the North Atlantic and **b)** the North Pacific from MODIS Aqua data [*NASA Ocean Biology Processing Group*, 2015] spanning January 2004 to January 2016, with contours of mean dynamic topography from CNES CLS09 [*Rio et al.*, 2011] overlaid using a contour interval of 5 cm. The zonal and meridional lines in **a)** show sections along which data will be extracted for comparison with the idealized modeling results.

We use the advection-diffusion equation in cylindrical co-ordinates with additional terms to represent the biogeochemical sinks and sources of phosphate. The model solves for an axisymmetric nutrient distribution that depends only on the distance from the center of the gyre. While this assumption ignores the dynamical asymmetry of western boundary currents and the scale difference between meridional and zonal directions, it can model the increase in chlorophyll concentration with distance from the center of the gyre, as seen in figure 2. The axisymmetric assumption removes the radial advection component from the advection-diffusion equation. Our idealized model parametrizes many processes that affect the distribution and concentration of nutrients. These are shown schematically in figure 3. The results of *Doddridge et al.* [2016] indicate that the residual Ekman circulation may be substantially different to the Eulerian-mean Ekman circulation, and that there is no Ekman downwelling through the base of the mode water layer. Our idealized model provides an efficient means of exploring the implications of reduced Ekman pumping, and the lack of Ekman driven downwelling through the thermocline, on the distribution of nutrients within subtropical gyres.

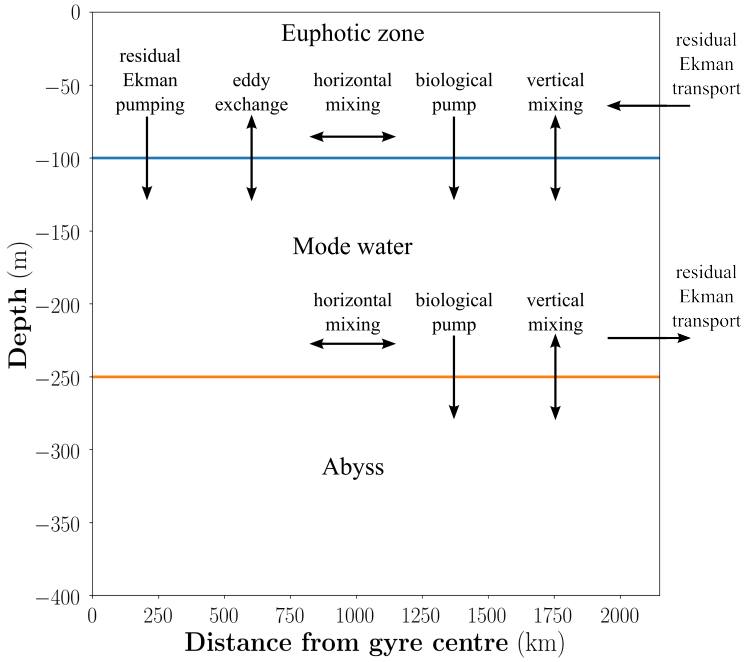

Figure 3. Schematic of the cylindrical co-ordinate model showing the two-layer domain and the processes included in the model.

Augmenting the advection-diffusion equation with the processes shown in figure 3 gives an equation for the concentration of phosphate in the euphotic zone with the form

$$
\begin{aligned}
h_{\text{euph}}\frac{\partial[PO_4]}{\partial t} = \frac{1}{r}\frac{\partial}{\partial r}\left(\kappa_h r h_{\text{euph}}\frac{\partial[PO_4]}{\partial r}\right) + \kappa_z\left(\frac{[PO_{4\text{mode}}]-[PO_4]}{h_{\text{euph}}}\right) \\
+ (w_{\text{Ek}}+\overline{w_{\text{eddy}}})[PO_4] - \frac{1}{2r}\frac{\partial((w_{\text{Ek}}+\overline{w_{\text{eddy}}})r^2[PO_4])}{\partial r} \\
- \alpha h_{\text{euph}} I_c \frac{[PO_4]}{[PO_4]+\lambda_{PO_4}} + h_{\text{euph}}\gamma_{\text{remin}}[DOP] \\
+ w_{\text{rms}} A_{\text{eddy}} E_{\text{eddy}}\left([PO_{4\text{mode}}]-[PO_4]\right),
\end{aligned}
\tag{1}
$$

in which h_{euph} is the thickness of the euphotic zone, $[PO_4]$ is the vertically averaged concentration of phosphate in the euphotic zone, κ_h is the horizontal diffusivity and parametrizes the horizontal mixing effects of eddies in the euphotic zone, κ_z is the vertical diffusivity, $[PO_{4\text{mode}}]$ is the vertically averaged concentration of phosphate in the mode water layer, w_{Ek} is the Eulerian-mean Ekman pumping velocity, $\overline{w_{\text{eddy}}}$ is the representative vertical velocity from eddy cancellation which opposes Ekman pumping, α is the maximum net community production, I_c represents the impact of light limitation and is set to one for the simulations in this paper, λ_{PO_4} is the half saturation concentration for phosphate, γ_{remin} is the remineralisation timescale for dissolved organic phosphate, $[DOP]$ is the vertically averaged concentration of dissolved organic phosphate in the euphotic zone, w_{rms} is the representative vertical velocity for eddy exchange between the two layers, A_{eddy} is the fraction of the ocean covered by eddies, and E_{eddy} is the efficiency of eddy pumping. The vertical mixing term represents the diffusive flux of phosphate between the two layers, and hence it is a first, rather than second, derivative. We include a horizontal mass flux, the

fourth term on the right hand side, to balance the vertical mass flux due to residual Ekman pumping, the third term on the right hand side.

As can be inferred from equation (1) the impact of eddies is parametrized in three ways in this idealized model:

- eddy cancellation is included through modification of the Ekman pumping velocity by $\overline{w_{\text{eddy}}}$, the key new effect considered in this contribution;
- horizontal stirring by eddies is parametrized through the horizontal mixing term [see e.g. *Lee and Williams*, 2000]; and
- the eddy pumping mechanism of *McGillicuddy and Robinson* [1997] and *McGillicuddy et al.* [1998, 2003] is parametrized as a vertical exchange of fluid between the two layers.

Because both eddy cancellation and eddy pumping both involve the vertical transport of nutrients, it may appear that an idealized model with both effects is double counting the impact of eddies. However, eddy pumping is an intrinsically adiabatic process that relies on the vertical motion of isopycnals, while eddy cancellation acts to reduce the diapycnal vertical motion observed in the Eulerian-mean velocity fields. As described by *Doddridge et al.* [2016], *Marshall* [2000], and *Polton and Marshall* [2003, 2007], the presence of strong residual downwelling in subtropical gyres is not consistent with an adiabatic ocean interior. Eddy pumping and eddy cancellation are two distinct processes and should both be represented in our idealized model. Since eddy pumping, as described by *McGillicuddy and Robinson* [1997] and *McGillicuddy et al.* [1998, 2003] is an intrinsically adiabatic process, our parametrization of it as an exchange of fluid between the two layers is somewhat awkward. However, unlike the thermocline, the base of the euphotic zone is defined by the abundance of light, not a density gradient, and in the clear waters of the subtropical gyres the euphotic zone is deeper than the mixed layer [p.268 *Williams and Follows*, 2011]. As such, the transfer of fluid from the mode water to the euphotic zone does not necessarily require a change in density.

The equation for the concentration of phosphate in the mode water layer is structurally similar, and takes the form

$$\begin{aligned} h_{\text{mode}}\frac{\partial[PO_{4\text{mode}}]}{\partial t} = {} & \frac{1}{r}\frac{\partial}{\partial r}\left(\kappa_h r h_{\text{mode}}\frac{\partial[PO_{4\text{mode}}]}{\partial r}\right) \\ & - \kappa_z\frac{[PO_{4\text{mode}}]-[PO_4]}{h_{\text{euph}}} + \kappa_z\frac{[PO_{4\text{abyss}}]-[PO_{4\text{mode}}]}{h_{\text{mode}}} \\ & - (w_{\text{Ek}}+\overline{w_{\text{eddy}}})[PO_4] + \frac{1}{2r}\frac{\partial((w_{Ek}+\overline{w_{\text{eddy}}})r^2[PO_{4\text{mode}}])}{\partial r} \\ & + (1-f_{DOP})\alpha h_{\text{euph}} I_c\frac{[PO_4]}{[PO_4]+\lambda_{PO_4}}\left(1-\left(\frac{h_{\text{mode}}+h_{\text{euph}}}{h_{\text{euph}}}\right)^{-0.988}\right) \\ & + h_{\text{mode}}\gamma_{\text{remin}}[DOP_{\text{mode}}] - w_{\text{rms}}A_{\text{eddy}}E_{\text{eddy}}\left([PO_{4\text{mode}}]-[PO_4]\right), \end{aligned} \tag{2}$$

in which

$$(1-f_{DOP})\alpha h_{\text{euph}} I_c\frac{[PO_4]}{[PO_4]+\lambda_{PO_4}}\left(1-\left(\frac{h_{\text{mode}}+h_{\text{euph}}}{h_{\text{euph}}}\right)^{-0.988}\right)$$

represents the particulate flux of organic matter that is remineralised in the mode water layer using the empirical power law derived by *Martin et al.* [1987], f_{DOP} is the fraction of productivity converted to dissolved organic phosphate, $[PO_{4\text{abyss}}]$ is the phosphate concentration in the abyssal ocean, and all other symbols have the same meanings as before.

These two equations are coupled with each other, and with two similar equations for dissolved organic phosphate (DOP). The equation for the concentration of DOP in the euphotic zone is

$$\begin{aligned} h_{\text{euph}}\frac{\partial[DOP]}{\partial t} = & \frac{1}{r}\frac{\partial}{\partial r}\left(\kappa_h r h_{\text{euph}}\frac{\partial[DOP]}{\partial r}\right) + \kappa_z\left(\frac{[DOP_{\text{mode}}]-[DOP]}{h_{\text{euph}}}\right) \\ & + (w_{Ek}+\overline{w_{\text{eddy}}})[DOP] - \frac{1}{2r}\frac{\partial((w_{\text{Ek}}+\overline{w_{\text{eddy}}})r^2[DOP])}{\partial r} \\ & + f_{\text{DOP}}\alpha h_{\text{euph}} I_c \frac{[PO_4]}{[PO_4]-\lambda_{PO_4}} \\ & - h_{\text{euph}}\gamma_{\text{remin}}[DOP] \\ & + w_{\text{rms}}A_{\text{eddy}}E_{\text{eddy}}\left([DOP_{\text{mode}}]-[DOP]\right), \end{aligned} \tag{3}$$

while the equation for the concentration of DOP in the mode water layer is

$$\begin{aligned} h_{\text{mode}}\frac{\partial[DOP_{\text{mode}}]}{\partial t} = & \frac{1}{r}\frac{\partial}{\partial r}\left(\kappa_h r h_{\text{mode}}\frac{\partial[DOP_{\text{mode}}]}{\partial r}\right) \\ & - \kappa_z\left(\frac{[DOP_{\text{mode}}]-[DOP]}{h_{\text{euph}}}\right) + \kappa_z\left(\frac{[DOP_{\text{abyss}}]-[DOP_{\text{mode}}]}{h_{\text{euph}}}\right) \\ & - (w_{\text{Ek}}+\overline{w_{\text{eddy}}})[DOP] \\ & + \frac{1}{2r}\frac{\partial((w_{\text{Ek}}+\overline{w_{\text{eddy}}})r^2[DOP_{\text{mode}}])}{\partial r} \\ & - h_{\text{mode}}\gamma_{\text{remin}}[DOP_{\text{mode}}] \\ & - w_{\text{rms}}A_{\text{eddy}}E_{\text{eddy}}\left([DOP_{\text{mode}}]-[DOP]\right). \end{aligned} \tag{4}$$

Together (1)-(4), form a set of coupled non-linear ordinary differential equations that we solve numerically. The solutions provide radial profiles of the concentration of phosphate and DOP in the euphotic zone and mode water layer. At the center of the gyre a zero-gradient boundary condition is enforced on all concentrations. At the gyre edge the concentration of phosphate and DOP in the euphotic zone is held at a fixed value chosen from climatological concentrations of phosphate [*Garcia et al.*, 2013] and DOP [*Torres-Valdés et al.*, 2009]. For phosphate and DOP in the mode water layer neither the concentration nor the radial gradient are prescribed at the gyre edge; the boundary value is obtained each time step by extrapolating half a grid point beyond the edge of the gyre using the gradient between the final two grid points. This allows the model to set the value and flux of these tracers at the boundary in a dynamically self-consistent manner.

We numerically solve these four coupled ordinary differential equations by integrating the equations for 1900 model years using an Adams-Bashforth third-order linear multi-step timestepping algorithm. The source code can be obtained from https://doddridge.me/publications/dm2018/.

2.1 Solutions using the default parameters

Solving the model with the default parameter values shown in table 1 produces the radial profiles of phosphate and dissolved organic phosphate concentration shown in figure 4. The model solutions have the same general shape as the climatological phosphate concentrations [*Garcia et al.*, 2013]. The solutions shown in figure 4 have not been tuned; the parameter values shown in table 1 were chosen on the basis of previous modeling and observational studies. Some of the parameter values, such as vertical diffusion and phosphate concentration at the edge of the gyre, are based on estimates derived from numerous observations. These parameters are therefore reasonably well constrained. However, other

parameters, such as the eddy cancellation velocity, are far more uncertain. As such, it is not clear what constitutes the "correct" value for these parameters. While it is possible to tune the parameters to make the model solutions more closely match the climatological profiles, the sensitivity of this model to variations in the parameters is of more interest than attempting to precisely reproduce the climatological profiles. As can be seen in figure 4 b), there is substantial variation between each of the observational phosphate transects from the mode water. The solution from our idealized model using the initial parameter values is also quite different from each of the observationally derived transects. This represents a shortcoming of our idealized model, and impacts the nutrient fluxes between the mode water and euphotic zone. However, it should be noted that the mode water phosphate concentration in our model is sensitive to a number of poorly constrained parameters, and that our focus is understanding the effect of these parameters on the nutrient distribution, not tuning our idealized model to exactly reproduce the observed distribution.

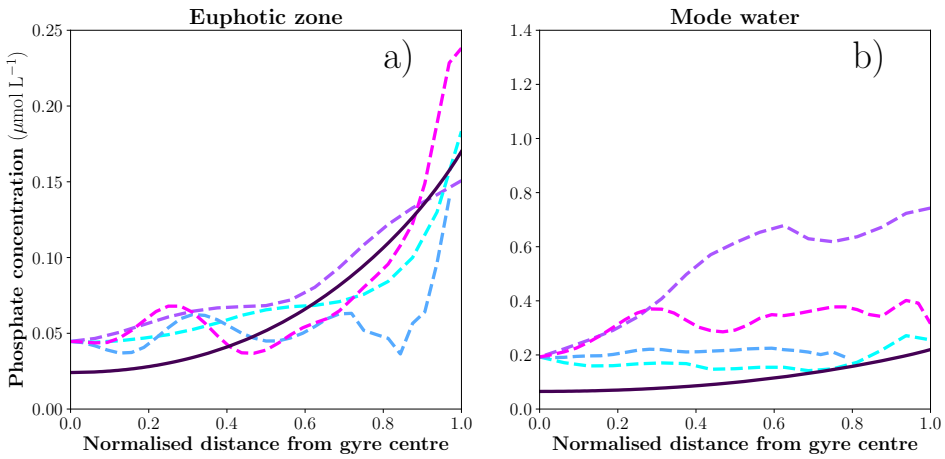

Figure 4. Solutions of the idealized model **a)** in the euphotic zone and **b)** in the mode water layer using the default parameters (solid line). The climatological phosphate concentrations from the subtropical North Atlantic [*Garcia et al.*, 2013] are shown for comparison (dashed lines) with colors matched to the sections indicated in figure 2 a). The mode water values are taken as the phosphate concentration on the 18.5 °C isotherm.

2.2 Nutrient budget of the idealized model

It is possible to construct a nutrient budget for the idealized model by considering the fluxes into and out of the domain. After integrating the model for 1900 years of model time the nutrient budget balances to approximately two parts in a thousand, as shown in table 2. Using the default parameters, shown in table 1, the largest source is the horizontal supply of nutrients by residual Ekman transport in to the euphotic zone, which provides 2.03×10^3 mol PO_4^{3-} s^{-1} through the horizontal advection of phosphate and 7.17×10^2 mol P s^{-1} through the horizontal advection of dissolved organic phosphate (DOP). Horizontal mixing also supplies some nutrients through the gyre edge in both layers, but this flux is much smaller than the horizontal Ekman flux. At a steady state most of the nutrients are removed from the domain by the horizontal residual Ekman transport in the mode water layer. The parametrized particulate flux also provides a sink of nutrients out of the domain.

258 **Table 1.** Default parameter values for the two layer advection-diffusion model.

Parameter	Symbol	Value	Units
Depth of euphotic zone	h_{euph}	100 [a]	m
Depth of mode water	h_{mode}	150 [b]	m
Maximum net community production	α	8.2×10^{-4} [c]	mol P m^{-3} year^{-1}
Fraction of production converted to dissolved organic phosphate (DOP)	f_{DOP}	0.67 [d]	
Remineralisation rate for DOP	γ_{remin}	2 [d]	year^{-1}
Phosphate half saturation	λ_{PO_4}	5×10^{-4} [d]	mol m^{-3}
Horizontal diffusion	κ_h	500 [e]	m^2 s^{-1}
Vertical diffusion	κ_z	1×10^{-5}	m^2 s^{-1}
Ekman pumping velocity	w_{Ek}	-80 [f]	m year^{-1}
Eddy cancellation velocity	$\overline{w_{\text{eddy}}}$	50 [g]	m year^{-1}
Light limitation coefficient	I_c	1	
Eddy pumping velocity	w_{rms}	1.0 [h]	m day^{-1}
Fractional area covered by eddies	A_{eddy}	0.2 [h]	
Eddy efficiency	E_{eddy}	0.4 [i]	
Phosphate concentration in euphotic zone at gyre edge		0.17×10^{-3} [j]	mol m^{-3}
DOP concentration in euphotic zone at gyre edge		0.06×10^{-3} [k]	mol m^{-3}
Abyssal phosphate concentration	$[PO_{4\text{abyss}}]$	0.5×10^{-3} [j]	mol m^{-3}
Gyre radius	R	2×10^{6} [l]	m

[a] based on previous modeling studies and observations [*Hemsley et al.*, 2015; *Lévy et al.*, 2012; *Martin and Pondaven*, 2003; *Oschlies and Garçon*, 1998; *Oschlies*, 2002b; *Williams and Follows*, 1998]

[b] consistent with figure 9

[c] from *McKinley et al.* [2004] for the subtropical North Atlantic

[d] default values from the idealized MITgcm biogeochemical model described in *Dutkiewicz et al.* [2005]

[e] from *Marshall et al.* [2006] and *Rypina et al.* [2012] for the subtropical open ocean

[f] estimated from scatterometer derived wind stress climatology [*Risien and Chelton*, 2008; *Risien*, 2011]

[g] chosen to mostly cancel the Eulerian-mean Ekman pumping, consistent with *Doddridge et al.* [2016]

[h] taken from *Brannigan* [2016] and *McGillicuddy* [2016]

[i] *Martin and Pondaven* [2003]

[j] estimated from the World Ocean Atlas climatology [*Garcia et al.*, 2013]

[k] estimated from DOP climatology [*Torres-Valdés et al.*, 2009]

[l] estimated from the size of the North Atlantic subtropical gyre

Table 2. Nutrient budget for the two layer advection-diffusion model integrated using the default parameter values from table 1.

Process	Nutrient flux (mol P s^{-1})
Residual Ekman transport (PO_4^{3-} in euphotic zone)	2.03×10^3
Residual Ekman transport (DOP in euphotic zone)	7.17×10^2
Horizontal mixing (PO_4^{3-} in euphotic zone)	1.32×10^2
Horizontal mixing (DOP in euphotic zone)	3.07
Residual Ekman transport (PO_4^{3-} in mode water layer)	-2.63×10^3
Residual Ekman transport (DOP in mode water layer)	-1.19×10^2
Horizontal mixing (PO_4^{3-} in mode water layer)	1.93×10^2
Horizontal mixing (DOP in mode water layer)	2.85
Vertical mixing (PO_4^{3-} from abyss to mode water layer)	3.06×10^2
Particulate flux through thermocline	-6.48×10^2
Sum	-8.51

2.3 Sensitivity testing

By varying the parameter values and rerunning our simplified model we are able to explore the parameter space and examine the effect of these parameter variations on the radial profile of phosphate. The sensitivity to residual Ekman pumping velocity is of particular interest following the results of *Doddridge et al.* [2016]. The sensitivity of our model to variations to the eddy pumping velocity, the residual Ekman pumping velocity, and the thickness of the mode water layer is shown in figure 5.

The eddy pumping mechanism proposed by *McGillicuddy and Robinson* [1997] is included in this model as a direct exchange of fluid between the mode water layer and the euphotic zone. As discussed by *Martin and Pondaven* [2003], eddy pumping is unlikely to be 100% efficient. When a water parcel is upwelled into the euphotic zone its nutrients are quickly consumed. After the water parcel is downwelled out of the euphotic zone, a finite amount of time is required for the nutrient concentration to return to its initial value. If subsequent mesoscale features return this water parcel to the euphotic zone before the nutrient concentration has recovered, the vertical nutrient flux due to eddy pumping will be reduced. Our idealized model represents this effect with an eddy pumping efficiency parameter, E_{eddy}, which we set to 40% based on *Martin and Pondaven* [2003]. Varying the eddy pumping velocity, w_{rms}, alters the steady-state phosphate concentration in the euphotic zone, with only a small change to the mode water concentration. However, this effect appears to saturate at large values of w_{rms}, with further increases in w_{rms} producing only small changes in the phosphate concentration in the euphotic zone and almost no change in the mode water layer, as shown in figure 5 a) and b). As noted by a reviewer, the biological uptake of phosphate is rapid compared with the rate of supply from below. This means that the productivity can continue to increase as the nutrient flux increases, even if the ambient nutrient concentration remains roughly the same.

Our simple model exhibits a non-monotonic response to changes in the residual Ekman pumping velocity, shown if figure 5 c) and d). For very small values of $w_{\text{Ek}} + \overline{w_{\text{eddy}}}$ the phosphate concentration decreases with increasing residual Ekman pumping. However, the response reverses sign at approximately 30 m year^{-1}, with subsequent increases in the residual Ekman pumping leading to increases in the phosphate concentration throughout the gyre. The value of 30 m year^{-1} is dependent on the parameter choices of the model, and should be considered suggestive, not authoritative. The initial decrease in phosphate concentration with small residual Ekman pumping velocities occurs because Ekman pump-

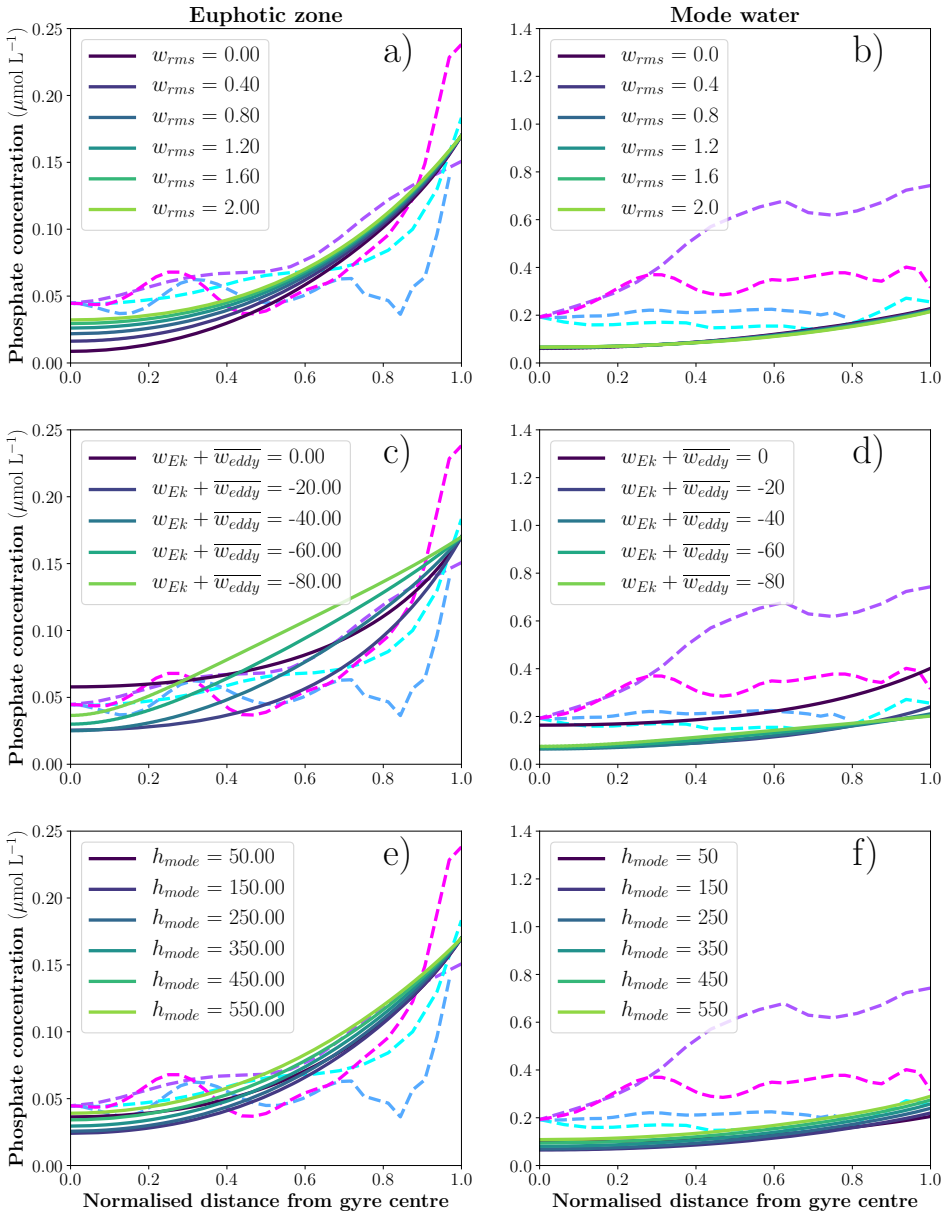

Figure 5. Sensitivity tests of the axisymmetric nutrient model for a range of parameter values. Each simulation varies only one parameter and uses the default parameter values shown in table 1 for all other parameters. **a)**, **c)** and **e)** show the nutrient distributions in the euphotic zone, while **b)**, **d)** and **f)** show the distributions in the mode water layer. **a)** and **b)** show the sensitivity to the eddy pumping velocity (w_{rms}), **c)** and **d)** show sensitivity to residual Ekman pumping velocity ($w_{\mathrm{Ek}} + \overline{w_{\mathrm{eddy}}}$), and **e)** and **f)** show the sensitivity to changes in the thickness of the mode water layer (h_{mode}).

ing moves nutrients from the euphotic zone into the mode water layer. For small residual pumping velocities the horizontal supply of nutrients is too small to compensate for this loss, especially near the center of the domain. The subsequent increase in productivity with increasing Ekman pumping is consistent with the horizontal Ekman transport of nutrients proposed by *Williams and Follows* [1998]. In our idealized model both phosphate and DOP are advected by the residual Ekman flow. If we define the area in our domain with nutrient concentration less than some threshold as oligotrophic, then, provided the residual Ekman pumping velocity is above 30 m year^{-1}, as the residual Ekman pumping increases in strength, the oligotrophic region within our domain shrinks. This is consistent with the observational results of *McClain et al.* [2004] who find that the size of the oligotrophic region of the Indian Ocean gyre decreases during periods of increased Ekman pumping. However, there are substantial differences between the analysis presented here and *McClain et al.* [2004], and comparisons should be evaluated with some skepticism. The analysis in *McClain et al.* [2004] used the time-varying Ekman pumping from the wind-stress curl, not the residual Ekman pumping velocity. The relationship between time-varying Ekman pumping and the residual Ekman pumping is not well understood. Recent work focusing on the Southern Ocean and Arctic suggests that the eddy response will likely take several years to respond to changes in the wind-stress [see e.g. *Davis et al.*, 2014; *Manucharyan and Spall*, 2016; *Sinha and Abernathey*, 2016]. This implies that seasonal variations in the wind-stress, like those analyzed by *McClain et al.* [2004], likely affect the residual velocity, but the exact relationship is unclear. Extending our idealized model to include a time-varying residual Ekman pumping velocity represents an exciting avenue for future work, but is beyond the scope of this contribution.

If eddy cancellation is as effective as the results of *Doddridge et al.* [2016] suggest, then we would expect the time-mean residual Ekman pumping velocity to be very small. As the residual Ekman pumping velocity decreases, the Ekman contribution to the nutrient budget also decreases. When $w_{\mathrm{Ek}} + \overline{w_{\mathrm{eddy}}}$ is zero the largest source of nutrients for the model is the horizontal diffusion of phosphate in the mode water layer. The nutrient budget for this simulation is shown in table 3. Despite integrating for 1900 years of model time, there is a 1.6% residual in the nutrient budget. The discrepancy in the nutrient budget in this simulation is larger than the simulation using the default parameters because the adjustment timescale is longer in the absence of Ekman driven advection.

Table 3. Nutrient budget for the two layer advection-diffusion model with $w_{\mathrm{Ek}} + \overline{w_{\mathrm{eddy}}}$ set to 0 m year^{-1}.

Process	Nutrient flux (mol P s^{-1})
Residual Ekman transport (PO_4^{3-} in euphotic zone)	0
Residual Ekman transport (DOP in euphotic zone)	0
Horizontal mixing (PO_4^{3-} in euphotic zone)	1.43×10^2
Horizontal mixing (DOP in euphotic zone)	2.57×10
Residual Ekman transport (PO_4^{3-} in mode water layer)	0
Residual Ekman transport (DOP in mode water layer)	0
Horizontal mixing (PO_4^{3-} in mode water layer)	3.45×10^2
Horizontal mixing (DOP in mode water layer)	3.75
Vertical mixing (PO_4^{3-} from abyss to mode water layer)	2.01×10^2
Particulate flux through thermocline	-7.31×10^2
Sum	-11.7

The sensitivity of our idealized model to changes in the mode water thickness is shown in figure 5 e) and f). *Palter et al.* [2005] suggest that the subtropical mode water layer reduces productivity in the subtropical gyres by introducing a wedge of low nutri-

ent water between the oligotrophic surface waters and the nutrient-rich abyss. *Palter et al.* [2005] hypothesize that higher than average mode water formation will inhibit productivity in subsequent years by increasing the thickness of this low nutrient wedge. Our idealized model suggests that this hypothesis holds for very thin mode water layers where the vertical diffusive flux of nutrients from the abyss is large. However, once the mode water thickness is above a critical value, thicker mode waters lead to higher productivity, as shown in figure 5 e) and f).

The non-monotonic response of nutrient concentration to mode water thickness in our model is the result of two competing processes. When the mode water layer is very thin, the vertical diffusive flux is able to transport more nutrients upwards into the gyre system from the nutrient rich abyss, as shown in figure 6 (left axis). As discussed by *Palter et al.* [2005], thicker mode water layers reduce the effectiveness of this mechanism. However, the thickness of the mode water layer also effects the efficiency of the biological pump: more of the parametrized particulate flux remineralises within a thicker mode water layer. This leads to more recycling of nutrients within the gyre system when the mode water layer is thick, and thus an increase in productivity. The fraction of the particulate flux that remineralises within the mode water layer of our idealized model is shown in figure 6 (right axis). Our idealized model simplifies the vertical dimension into two homogeneous layers, the euphotic zone and the mode water layer. This means that any phosphate remineralised within the mode water is evenly distributed throughout the depth of the mode water, which may cause our idealized model to overestimate the impact of remineralisation within the mode water on productivity.

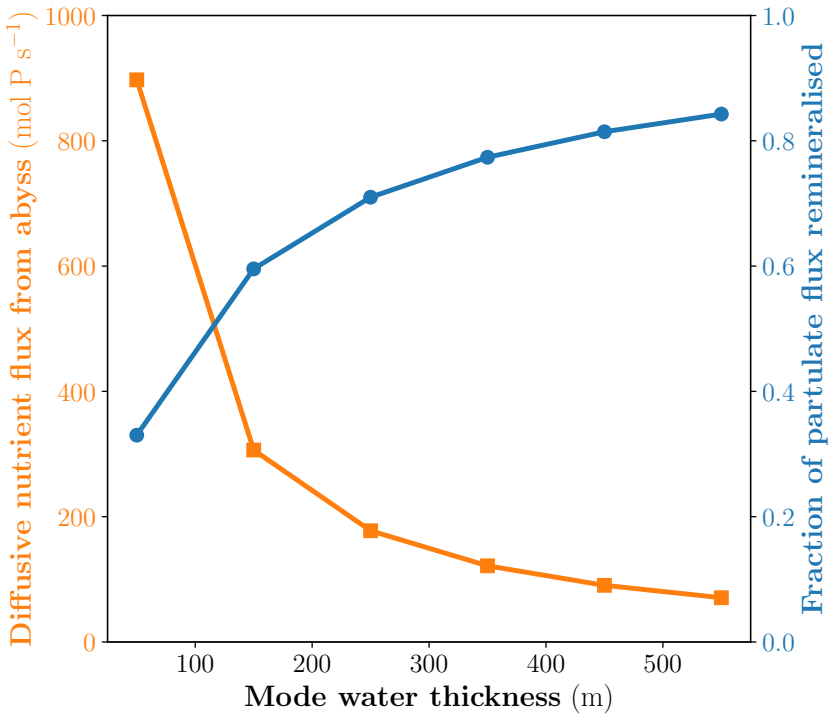

Figure 6. The diffusive flux of nutrient upwards from the abyss (left axis) and the fraction of the particulate flux that remineralises within the mode water layer (right axis). Both depend strongly on the thickness of the mode water layer. A thicker mode water layer leads to a lower nutrient supply from the abyss and more efficient recycling of nutrients within the gyre system.

Since the parameterized particulate flux is the only sink of nutrients in the simulation with zero residual Ekman pumping, as shown in table 3, we expect the sensitivity of the model to mode water thickness to strongly depend on the residual Ekman pumping velocity. For simulations with no residual Ekman pumping, we expect substantial sensitivity to mode water thickness, and when residual Ekman pumping is large, we expect little sensitivity to mode water thickness. Figure 7 shows the results from two additional sensitivity tests. Figure 7 a) includes no residual Ekman pumping, while figure 7 b) has $w_{Ek} + \overline{w_{eddy}}$ set to -80 m year^{-1}. As expected, the simulation with no residual Ekman pumping exhibits substantial sensitivity to the thickness of the mode water layer, while the simulation with a large residual Ekman pumping velocity is almost insensitive to this parameter. This may provide an indirect method to examine the residual Ekman pumping velocity in the observations: a relationship between mode water thickness and productivity is consistent with a small residual Ekman pumping velocity, and thus with eddy cancellation of the Eulerian-mean Ekman pumping.

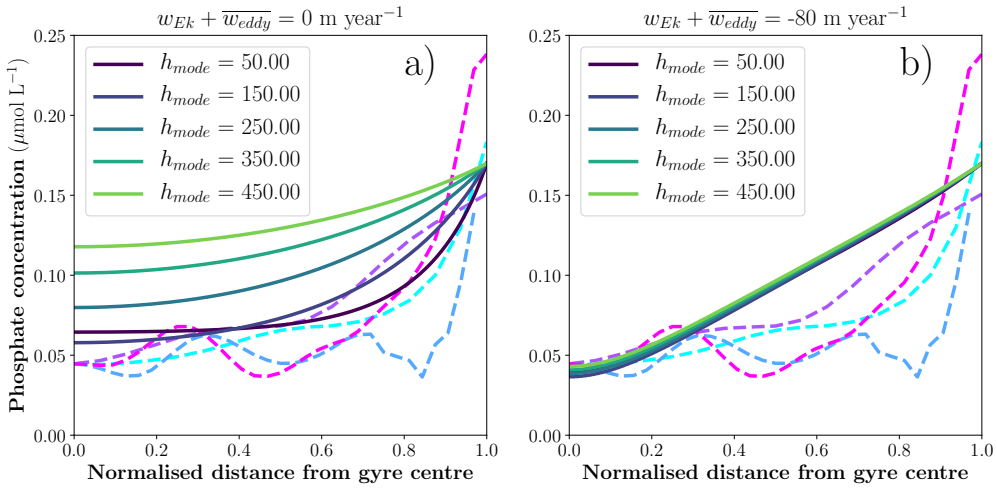

Figure 7. The sensitivity of our idealized model to mode water thickness depends on the residual Ekman pumping velocity. **a)** shows the solutions for $w_{Ek} + \overline{w_{eddy}}$ = 0 m year^{-1}, and **b)** for $w_{Ek} + \overline{w_{eddy}}$ = -80 m year^{-1}.

3 Analysis of observations

We now use observations to evaluate the predictions of our simple model. While observational estimates of the wind stress would allow us to calculate the Ekman pumping velocity, the results of *Doddridge et al.* [2016] suggest that the residual Ekman pumping velocity will differ substantially from this estimate. Furthermore, *Doddridge et al.* [2016] describe an equilibrium response and it is unclear how temporal variation of the Ekman pumping will affect the residual velocity. In the absence of an observational estimate for the residual Ekman pumping velocity, we focus on the influence of mode water thickness on productivity. As discussed previously, this also provides an indirect method to assess the residual Ekman pumping velocity; a dependence of productivity on mode water thickness is consistent with a small residual Ekman pumping velocity.

Palter et al. [2005] predict that a thicker mode water layer will inhibit productivity by reducing the vertical diffusive flux of nutrients from the abyss upwards into the euphotic zone. The influence of mode water on primary productivity was also explored by *Krémeur et al.* [2009], who concluded that the nutrient content of subtropical mode water

affected primary productivity in the subpolar region and the subtropical western boundary current, but had little influence over productivity within the gyre. Our idealized model predicts that, above some critical value, a thicker mode water layer will support higher productivity. In this section, we set out to test these three incompatible predictions using the observations.

3.1 Argo and satellite data

Worthington [1958] describe a volume of weakly stratified fluid that can be found across much of the North Atlantic. This water mass is known as eighteen degree water and is the mode water of the North Atlantic subtropical gyre. We estimate mode water thickness using a one-degree gridded Argo product: a continuation of the dataset described by *Roemmich and Gilson* [2009]. The relationship between potential temperature and salinity in mode waters is very robust [*Fratantoni et al.*, 2013], which means that the potential temperature field alone is adequate for diagnosing the mode water. Recent definitions of eighteen degree water include a vertical stratification criterion [*Alfultis and Cornillon*, 2001; *Klein and Hogg*, 1996; *Kwon and Riser*, 2004] as well as a temperature range. For the calculations presented here, the thickness of the North Atlantic subtropical mode water is determined as the difference in depth between the 17.5°C and 19°C isotherms. The choice of 17.5°C and 19°C was informed by the stratification minimum shown in figure 8. Our calculation of mode water thickness ignores the vertical gradient criterion used by *Klein and Hogg* [1996] and *Alfultis and Cornillon* [2001]. The vertical gradient criterion is ignored since the stratification minimum is slowly eroded as the mode water is advected southwards in the gyre [*Palter et al.*, 2005] and we wish to capture the thickness of these older mode water masses in the diagnostic. Figure 9 shows the Eulerian-mean mode water thickness over the subtropical North Atlantic and the ellipse within which the observational quantities are averaged.

Primary productivity within the North Atlantic subtropical gyre is taken from a satellite derived dataset [*O'Malley*, 2016]. This dataset is produced using the Vertically Generalized Production Model of *Behrenfeld and Falkowski* [1997] and satellite derived estimates of chlorophyll concentration [*NASA Ocean Biology Processing Group*, 2015] to estimate ocean primary productivity. The algorithm presented by *Behrenfeld and Falkowski* [1997] uses a temperature dependent function to convert satellite chlorophyll retrievals in to an estimate of primary productivity. Their algorithm was able to explain 86% of the variability of *in-situ* measurements of productivity obtained using carbon-14 fixation.

We spatially average primary productivity and mode water thickness within the area outlined by the black ellipse in figure 9, and then temporally average to obtain an annual average for each year in the time series. Figure 10 shows the spatially and temporally averaged quantities plotted against each other and the linear fit obtained from ordinary least squares regression of the data. While the slope of the regression line is positive and the linear fit explains approximately 18 % of the variance in primary productivity, the fit is not statistically significant ($p \approx 0.17$). Repeating the analysis averaging over different regions within the gyre produces similar non-significant results.

3.2 Bermuda Atlantic Time Series

The Bermuda Atlantic Time Series (BATS) provides a longer record of primary productivity and hydrography at approximately 32N, 64W in the Atlantic ocean. Additionally, rather than relying on satellite derived estimates of primary productivity, the BATS data are *in-situ* productivity measurements.

While the BATS data provide a unique co-located time series of *in-situ* primary productivity and hydrography measurements, these measurements are located towards the edge of the oligotrophic region of the North Atlantic. Furthermore, unlike the Argo and

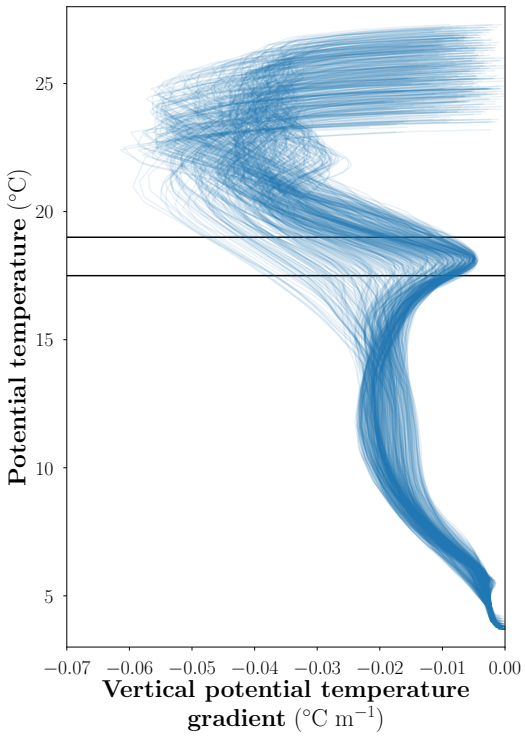

Figure 8. Profiles of vertical potential temperature gradient plotted against potential temperature for each one degree box within the ellipse shown in figure 9 using the Eulerian-mean potential temperature field for the period 2004 to 2015 [*Roemmich and Gilson*, 2009]. The stratification minimum within the mode water can be clearly seen at approximately 18 °C. The horizontal lines are at 17.5°C and 19°C, and are used to define the vertical extent of the mode water.

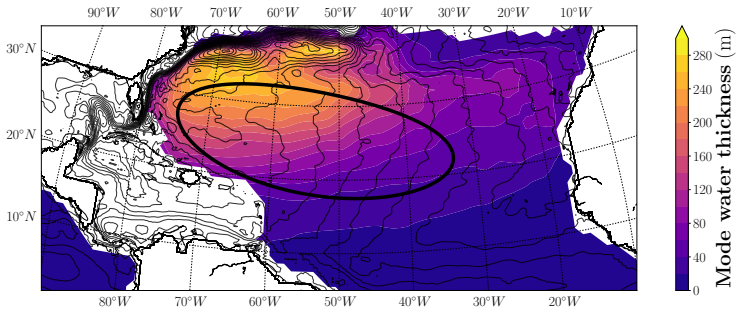

Figure 9. Eulerian-mean mode water thickness (m) in the North Atlantic subtropical region diagnosed as the depth difference between the 17.5°C and 19°C isotherms in the 2004-2015 Eulerian-mean temperature field. Unless both isotherms exist at a given grid point, that location is masked and shown in white. The thin black lines are contours of mean dynamic topography from CNES CLS09 [*Rio et al.*, 2011] in 5 cm intervals and the thick black ellipse shows the area over which the observational quantities are averaged.

satellite data, the BATS data come from a single location. This means that local effects, which may have been smeared out in the Argo and satellite data, could make a substantial contribution to our analysis. As such, this dataset might not accurately represent the

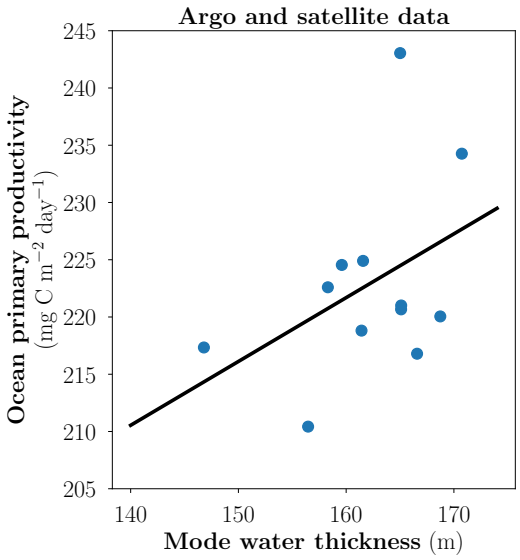

Figure 10. Annual mean ocean productivity (mg C m^{-2} day^{-1}) plotted against annual mean mode water thickness (m). Each quantity has been averaged over the ellipse shown in figure 9. The black line shows the ordinary least squares regression fit to the data. The slope is not significantly different from zero ($p \approx 0.17$).

behavior of the oligotrophic region in the center of the subtropical gyre. However, in the absence of a more appropriately located dataset, we analyze the BATS dataset.

We vertically integrate the primary productivity using the trapezoidal rule to yield primary productivity per unit area, rather than per unit volume. We deal with a single point of missing data within each cast by linearly interpolating between the adjacent values. If two adjacent measurements are missing, we do not use the data from that cast. We then search for CTD casts within ± 1 day and ± 30 km of the productivity measurements and compute the mode water thickness as the vertical distance between the 17.5°C and 19°C isotherms. If multiple casts are found, the thickness is computed for each individually, and then these thicknesses are averaged. Altering the temporal or spatial cutoffs for selecting CTD casts has only a minimal impact on the results (not shown). Performing a regression analysis on this dataset shows a statistically significant linear relationship between mode water thickness and primary productivity ($p \approx 0.033$) that explains 1.5% of the variance in primary productivity (not shown). However, the mechanism by which we expect mode water thickness to affect primary productivity is an equilibrium mechanism, and so we bin the data into yearly averages. Performing a regression on the annually averaged data, shown in figure 11, again finds a statistically significant linear relationship ($p \approx 0.027$), but now mode water thickness explains 19.5% of the variance in primary productivity. This analysis supports our hypothesis that a thicker mode water layer leads to higher primary productivity, and that this effect operates over a long timescale.

4 Limitations

The idealized model and observational analyses we present suffer from a range of limitations. Our simple model solves for a radially symmetric distribution of nutrients, but in reality subtropical gyres are not circular. By assuming radial symmetry our model excludes any effects of western boundary currents on nutrient concentration. In both of the observational analyses, the observational record is relatively short for examining an equilibrium mechanism. Additionally, both the mode water thickness field, shown in figure 9,

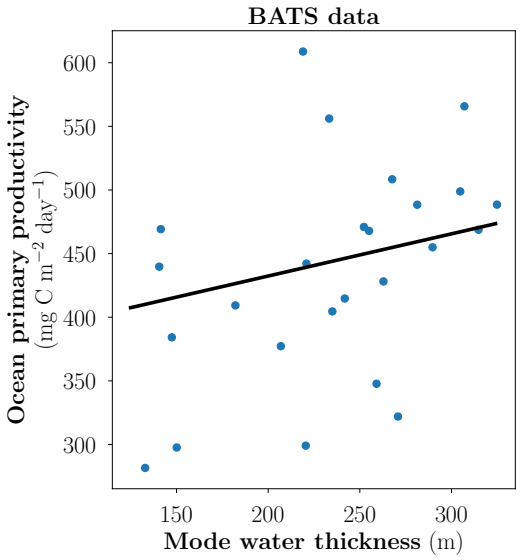

Figure 11. Annually averaged data from the Bermuda Atlantic Time Series (BATS) and the statistically significant ($p \approx 0.027$) linear fit between mode water thickness and primary productivity, which explains 19.5% of the variance in primary productivity.

and primary productivity contain strong meridional gradients. In our gyre-scale analysis the northern edge of the ellipse occupies a region with thicker mode water and higher productivity, while the southern edge is in a region with thinner mode water and lower productivity. By averaging the mode water thickness and estimated productivity over a large region we are explicitly discarding any spatial structure in the response. In our idealized model the effect of mode water thickness on phosphate concentration is strongest in the center, since the edges are held fixed at the observed phosphate concentration. Because we are interested in the effect of mode water thickness on productivity in the oligotrophic region of the gyre we have attempted to keep our analysis region away from the boundary of the gyre.

The BATS data were collected in a region in which mode water thickness and primary productivity both decrease to the south and increase to the north. This means that meridional excursions of the gyre could cause our observational estimates of mode water thickness and productivity to co-vary. This could potentially contaminate the results and strengthen the observed relationship between mode water thickness and productivity. Despite these significant limitations it is encouraging that statistically significant relationships emerge that broadly support the predictions of the idealized model.

5 Concluding remarks

The nutrient budget for the oligotrophic subtropical gyres remains uncertain. In this paper we have presented an idealized model for phosphate concentration in subtropical gyres that includes the previously unconsidered process of eddy cancellation. Our idealized model qualitatively reproduces the observed nutrient concentrations. To test our understanding of the processes that set the nutrient concentrations, we have explored the sensitivity of this model to variations in the parameter values.

Increasing the eddy pumping velocity, w_{eddy}, in our idealized model leads to increased productivity. However, as the strength of the eddy pumping is increased, the sen-

sitivity of our model to eddy pumping decreases. When the eddy pumping parameter is large, increases in the parameter produce a smaller effect than when there is little eddy pumping. This result from our idealized model is similar to the findings presented by *Lévy et al.* [2012] and suggests that the efficacy of eddy pumping is strongly bounded from above.

Our idealized model responds non-monotonically to variations in the residual Ekman pumping velocity. Initially, increasing Ekman pumping suppresses productivity, however, above a certain value increasing the residual Ekman pumping velocity leads to additional productivity. This increase in productivity is due to the horizontal flux of nutrients into the gyre and is consistent with *McClain et al.* [2004] and *Williams and Follows* [1998]. The sensitivity of our idealized model to the residual Ekman pumping velocity suggests that eddy cancellation may play an important role in setting nutrient concentrations in subtropical gyres.

Contrary to the hypothesis proposed by *Palter et al.* [2005] we find that increased mode water thickness leads to increased productivity for all but the thinnest mode water layers. A thicker mode water layer reduces the particulate flux of nutrients through the thermocline, thereby reducing the effectiveness of the biological pump. This leads to more nutrient recycling within the gyre, and thus, higher productivity. In our idealized model the impact of mode water thickness on nutrient concentration, and therefore productivity, is dependent on the residual Ekman pumping velocity. The observed relationship between mode water thickness and productivity is consistent with a small residual Ekman pumping velocity, and therefore highly effective eddy cancellation, in the subtropical North Atlantic gyre. While the data are somewhat noisy, the underlying dynamical mechanism is based on a robust physical argument supported by detailed eddy-resolving model calculations. In combination with the results of *Doddridge et al.* [2016] the results presented here suggest that oligotrophic subtropical gyres may recycle nutrients much more effectively than has previously been thought.

Acknowledgments

We are grateful to Adrian Martin, Helen Johnson, and two anonymous reviewers for their insightful comments.

EWD received financial support from The Rhodes Trust, Magdalen College Oxford, the Vice-Chancellor's Fund of Oxford University, and Atmospheric Oceanic & Planetary Physics Oxford. DPM acknowledges the support of the UK Natural Environment Research Council (NE/R000999/1)

Satellite derived productivity dataset can be downloaded from
http://www.science.oregonstate.edu/ocean.productivity/index.php

The gridded Argo dataset can be downloaded from
http://sio-argo.ucsd.edu/RG_Climatology.html

The Bermuda Atlantic Time Series productivity data can be downloaded from
http://batsftp.bios.edu/BATS/production/
and the CTD data from
http://batsftp.bios.edu/BATS/ctd/

The source code for our idealized model and the analyses described in this manuscript can be found here: https://doddridge.me/publications/dm2018/

References

Alfultis, M. a., and P. Cornillon (2001), Annual and Interannual Changes in the North Atlantic STMW Layer Properties, *J. Phys. Oceanogr.*, *31*(8), 2066–2086, doi:10.1175/1520-0485(2001)031<2066:AAICIT>2.0.CO;2.

Behrenfeld, M. J., and P. G. Falkowski (1997), Photosynthetic rates derived from satellite-based chlorophyll concentration, *Limnol. Oceanogr.*, *42*(1), 1–20, doi:10.4319/lo.1997.42.1.0001.

Brannigan, L. (2016), Intense submesoscale upwelling in anticyclonic eddies, *Geophys. Res. Lett.*, *43*(7), 3360–3369, doi:10.1002/2016GL067926.

Burkholder, K. C., and M. S. Lozier (2014), Tracing the pathways of the upper limb of the North Atlantic Meridional Overturning Circulation, *Geophys. Res. Lett.*, *41*(12), 4254–4260, doi:10.1002/2014GL060226.

Davis, P. E. D., C. Lique, and H. L. Johnson (2014), On the link between arctic sea ice decline and the freshwater content of the beaufort gyre: Insights from a simple process model, *J. Clim.*, *27*(21), 8170–8184, doi:10.1175/JCLI-D-14-00090.1.

Doddridge, E. W., D. P. Marshall, and A. M. Hogg (2016), Eddy Cancellation of the Ekman Cell in Subtropical Gyres, *J. Phys. Oceanogr.*, *46*(10), 2995–3010, doi:10.1175/JPO-D-16-0097.1.

Dutkiewicz, S., A. P. Sokolov, J. Scott, and P. H. Stone (2005), A Three-Dimensional Ocean-Seaice-Carbon Cycle Model and its Coupling to a Two-Dimensional Atmospheric Model: Uses in Climate Change Studies, *Tech. Rep. 122*.

Fratantoni, D. M., Y.-O. Kwon, and B. A. Hodges (2013), Direct observation of subtropical mode water circulation in the western North Atlantic Ocean, *Deep Sea Res. Part II Top. Stud. Oceanogr.*, *91*, 35–56, doi:10.1016/j.dsr2.2013.02.027.

Garcia, H. E., R. A. Locarnini, T. P. Boyer, J. I. Antonov, O. K. Baranova, M. M. Zweng, J. Reagan, and D. R. Johnson (2013), World Ocean Atlas 20013 Volume 4: Dissolved Inorganic Nutrients (phosphate, nitrate, silicate), *Tech. Rep. September*, doi:10.1182/blood-2011-06-357442.

Hemsley, V. S., T. J. Smyth, A. P. Martin, E. Frajka-Williams, A. F. Thompson, G. Damerell, and S. C. Painter (2015), Estimating Oceanic Primary Production Using Vertical Irradiance and Chlorophyll Profiles from Ocean Gliders in the North Atlantic, *Environ. Sci. Technol.*, *49*(19), 11,612–11,621, doi:10.1021/acs.est.5b00608.

Jenkins, W. J. (1982), Oxygen utilization rates in North Atlantic subtropical gyre and primary production in oligotrophic systems, *Nature*, *300*(5889), 246–248, doi:10.1038/300246a0.

Jenkins, W. J., and S. C. Doney (2003), The subtropical nutrient spiral, *Global Biogeochem. Cycles*, *17*(4), doi:10.1029/2003GB002085.

Klein, B., and N. G. Hogg (1996), On the variability of 18 Degree Water formation as observed from moored instruments at 55W, *Deep Sea Res. Part I Oceanogr. Res. Pap.*, *43*(11-12), 1777–1806, doi:10.1016/S0967-0637(96)00069-6.

Krémeur, A.-S., M. Lévy, O. Aumont, and G. Reverdin (2009), Impact of the subtropical mode water biogeochemical properties on primary production in the North Atlantic: New insights from an idealized model study, *J. Geophys. Res.*, *114*(C7), C07,019, doi:10.1029/2008JC005161.

Kwon, Y. O., and S. C. Riser (2004), North Atlantic subtropical mode water: A history of ocean-atmosphere interaction 1961-2000, *Geophys. Res. Lett.*, *31*(19), 1–4, doi:10.1029/2004GL021116.

Lee, M.-M., and R. G. Williams (2000), The role of eddies in the isopycnic transfer of nutrients and their impact on biological production, *J. Mar. Res.*, *58*(6), 895–917, doi:10.1357/002224000763485746.

Letscher, R. T., F. Primeau, and J. K. Moore (2016), Nutrient budgets in the subtropical ocean gyres dominated by lateral transport, *Nat. Geosci.*, *9*(11), 815–819, doi:10.1038/ngeo2812.

Lévy, M. (2008), The Modulation of Biological Production by Oceanic Mesoscale Turbulence, in *Transp. Mix. Geophys. Flows*, vol. 744, edited by J. B. Weiss and A. Provenzale, pp. 219–261, Springer, Berlin.

Lévy, M., D. Iovino, L. Resplandy, P. Klein, G. Madec, A.-M. Tréguier, S. Masson, and K. Takahashi (2012), Large-scale impacts of submesoscale dynamics on phytoplankton: Local and remote effects, *Ocean Model.*, *43-44*, 77–93, doi: 10.1016/j.ocemod.2011.12.003.

Manucharyan, G. E., and M. A. Spall (2016), Wind-driven freshwater buildup and release in the Beaufort Gyre constrained by mesoscale eddies, *Geophys. Res. Lett.*, *43*(1), 273–282, doi:10.1002/2015GL065957.

Marshall, D. P. (2000), Vertical Fluxes of Potential Vorticity and the Structure of the Thermocline, *J. Phys. Oceanogr.*, *30*(12), 3102–3112, doi:10.1175/1520-0485(2000)030<3102:VFOPVA>2.0.CO;2.

Marshall, J., E. Shuckburgh, H. Jones, and C. Hill (2006), Estimates and Implications of Surface Eddy Diffusivity in the Southern Ocean Derived from Tracer Transport, *J. Phys. Oceanogr.*, *36*(9), 1806–1821, doi:10.1175/JPO2949.1.

Martin, A. P., and P. Pondaven (2003), On estimates for the vertical nitrate flux due to eddy pumping, *J. Geophys. Res.*, *108*(C11), 3359, doi:10.1029/2003JC001841.

Martin, J. H., G. A. Knauer, D. M. Karl, and W. W. Broenkow (1987), VERTEX: carbon cycling in the northeast Pacific, *Deep Sea Res. Part A. Oceanogr. Res. Pap.*, *34*(2), 267–285, doi:10.1016/0198-0149(87)90086-0.

McClain, C. R., S. R. Signorini, and J. R. Christian (2004), Subtropical gyre variability observed by ocean-color satellites, *Deep Sea Res. Part II Top. Stud. Oceanogr.*, *51*(1-3), 281–301, doi:10.1016/j.dsr2.2003.08.002.

McGillicuddy, D., and A. Robinson (1997), Eddy-induced nutrient supply and new production in the Sargasso Sea, *Deep Sea Res. Part I Oceanogr. Res. Pap.*, *44*(8), 1427–1450, doi:10.1016/S0967-0637(97)00024-1.

McGillicuddy, D. J. (2016), Mechanisms of Physical-Biological-Biogeochemical Interaction at the Oceanic Mesoscale, *Ann. Rev. Mar. Sci.*, *8*(1), 125–159, doi:10.1146/annurev-marine-010814-015606.

McGillicuddy, D. J., A. R. Robinson, D. a. Siegel, H. W. Jannasch, R. Johnson, T. D. Dickey, J. McNeil, A. F. Michaels, and A. H. Knap (1998), Influence of mesoscale eddies on new production in the Sargasso Sea, *Nature*, *394*(6690), 263–266, doi: 10.1038/28367.

McGillicuddy, D. J., L. a. Anderson, S. C. Doney, and M. E. Maltrud (2003), Eddy-driven sources and sinks of nutrients in the upper ocean: Results from a 0.1 degree resolution model of the North Atlantic, *Global Biogeochem. Cycles*, *17*(2), doi: 10.1029/2002GB001987.

McKinley, G. A., M. J. Follows, and J. C. Marshall (2004), Mechanisms of air-sea CO2 flux variability in the equatorial Pacific and the North Atlantic, *Global Biogeochem. Cycles*, *18*(2), 1–14, doi:10.1029/2003GB002179.

NASA Ocean Biology Processing Group (2015), MODIS-Aqua Level 3 Mapped Chlorophyll Data Version 2014, doi:10.5067/AQUA/MODIS/L3M/CHL/2014.

O'Malley, R. (2016), Ocean Productivity, http://www.science.oregonstate.edu/ocean.productivity/index.php.

Oschlies, A. (2002a), Nutrient supply to the surface waters of the North Atlantic: A model study, *J. Geophys. Res.*, *107*(C5), 3046, doi:10.1029/2000JC000275.

Oschlies, A. (2002b), Can eddies make ocean deserts bloom?, *Global Biogeochem. Cycles*, *16*(4), 53–1–53–11, doi:10.1029/2001GB001830.

Oschlies, A., and V. Garçon (1998), Eddy-induced enhancement of primary production in a model of the North Atlantic Ocean, *Nature*, *394*(6690), 266–269, doi:10.1038/28373.

Palter, J. B., M. S. Lozier, and R. T. Barber (2005), The effect of advection on the nutrient reservoir in the North Atlantic subtropical gyre, *Nature*, *437*(7059), 687–692, doi: 10.1038/nature03969.

Pelegrí, J., A. Marrero-Díaz, and A. Ratsimandresy (2006), Nutrient irrigation of the North Atlantic, *Prog. Oceanogr.*, *70*(2-4), 366–406, doi:10.1016/j.pocean.2006.03.018.

Polton, J. A., and D. P. Marshall (2003), Understanding the Structure of the Subtropical Thermocline, *J. Phys. Oceanogr.*, *33*(6), 1240–1249, doi:10.1175/1520-0485(2003)033<1240:UTSOTS>2.0.CO;2.

Polton, J. A., and D. P. Marshall (2007), Overturning cells in the Southern Ocean and subtropical gyres, *Ocean Sci.*, *3*(1), 17–30, doi:10.5194/os-3-17-2007.

Rio, M. H., S. Guinehut, and G. Larnicol (2011), New CNES-CLS09 global mean dynamic topography computed from the combination of GRACE data, altimetry, and in situ measurements, *J. Geophys. Res.*, *116*(C7), C07,018, doi:10.1029/2010JC006505.

Risien, C. M. (2011), Scatterometer Climatology of Ocean Winds - SCOW, *http://cioss.coas.oregonstate.edu/scow/index.html*.

Risien, C. M., and D. B. Chelton (2008), A Global Climatology of Surface Wind and Wind Stress Fields from Eight Years of QuikSCAT Scatterometer Data, *J. Phys. Oceanogr.*, *38*(11), 2379–2413, doi:10.1175/2008JPO3881.1.

Roemmich, D., and J. Gilson (2009), The 2004-2008 mean and annual cycle of temperature, salinity, and steric height in the global ocean from the Argo Program, *Prog. Oceanogr.*, *82*(2), 81–100, doi:10.1016/j.pocean.2009.03.004.

Rypina, I. I., I. Kamenkovich, P. Berloff, and L. J. Pratt (2012), Eddy-Induced Particle Dispersion in the Near-Surface North Atlantic, *J. Phys. Oceanogr.*, *42*(12), 2206–2228, doi:10.1175/JPO-D-11-0191.1.

Siegel, D. A., D. J. McGillicuddy, and E. A. Fields (1999), Mesoscale eddies, satellite altimetry, and new production in the Sargasso Sea, *J. Geophys. Res. Ocean.*, *104*(C6), 13,359–13,379, doi:10.1029/1999JC900051.

Sinha, A., and R. P. Abernathey (2016), Time Scales of Southern Ocean Eddy Equilibration, *J. Phys. Oceanogr.*, *46*(9), 2785–2805, doi:10.1175/JPO-D-16-0041.1.

Torres-Valdés, S., V. M. Roussenov, R. Sanders, S. Reynolds, X. Pan, R. Mather, A. Landolfi, G. A. Wolff, E. P. Achterberg, and R. G. Williams (2009), Distribution of dissolved organic nutrients and their effect on export production over the Atlantic Ocean, *Global Biogeochem. Cycles*, *23*(4), 1–16, doi:10.1029/2008GB003389.

Williams, R. G., and M. J. Follows (1998), The Ekman transfer of nutrients and maintenance of new production over the North Atlantic, *Deep Sea Res. Part I Oceanogr. Res. Pap.*, *45*(2-3), 461–489, doi:10.1016/S0967-0637(97)00094-0.

Williams, R. G., and M. J. Follows (2011), *Ocean Dynamics and the Carbon Cycle: Principles and Mechanisms*, 416 pp., Cambridge University Press, Cambridge, UK.

Williams, R. G., V. Roussenov, and M. J. Follows (2006), Nutrient streams and their induction into the mixed layer, *Global Biogeochem. Cycles*, *20*(1), GB1016, doi:10.1029/2005GB002586.

Worthington, L. (1958), The 18° water in the Sargasso Sea, *Deep Sea Res.*, *5*(2-4), 297–305, doi:10.1016/0146-6313(58)90026-1.

Figure 1.

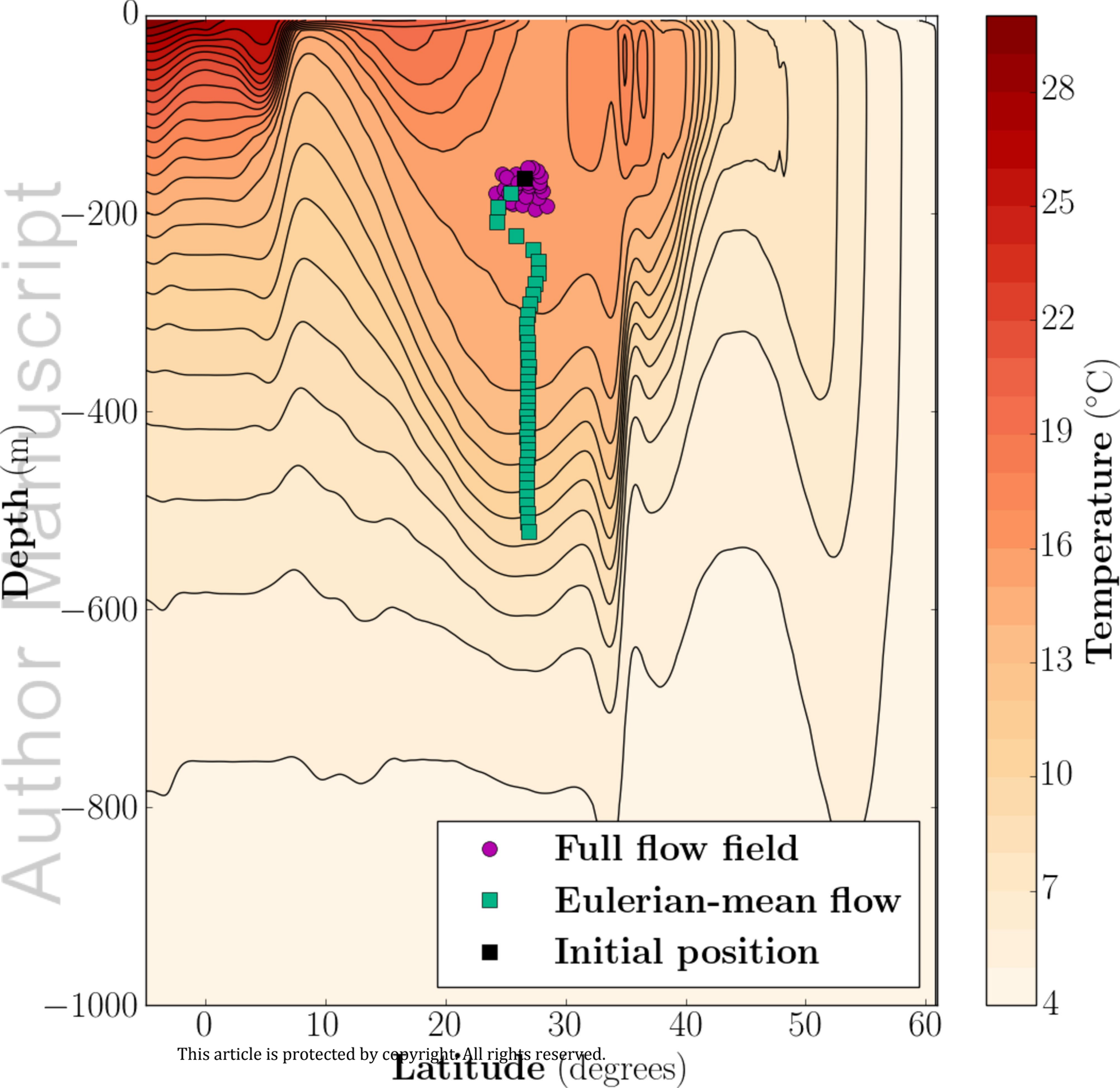

Figure 2.

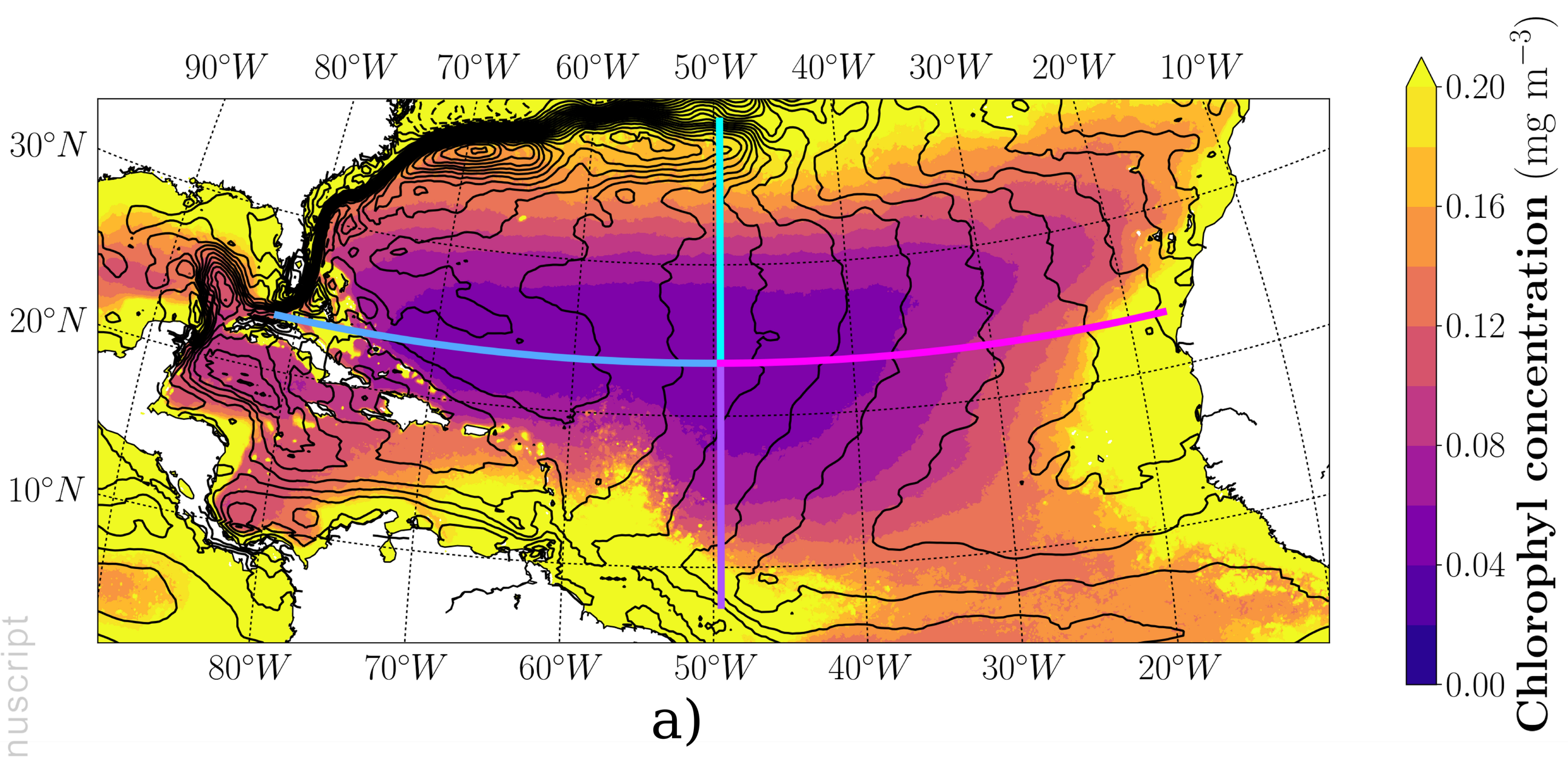

a)

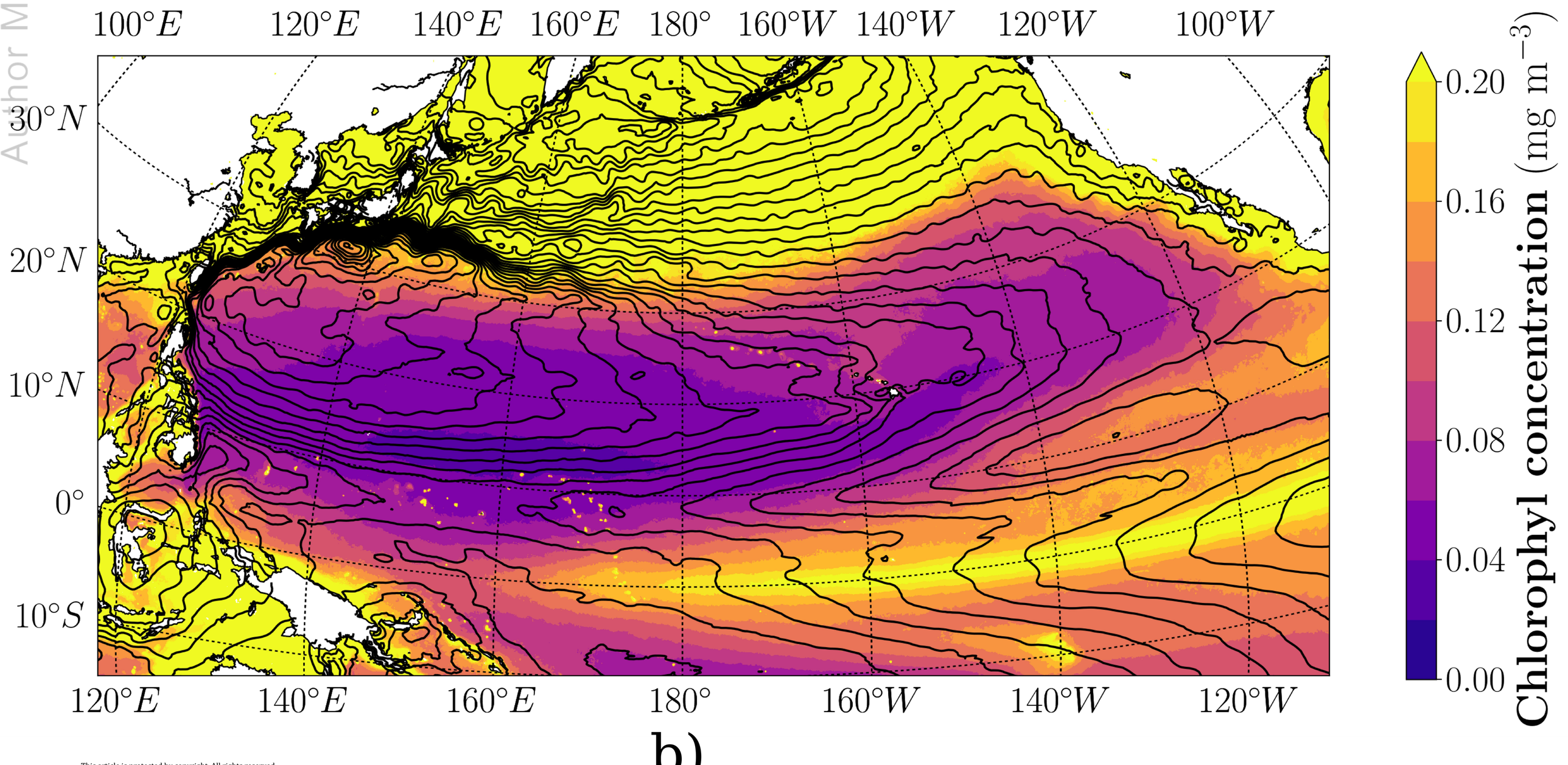

b)

Figure 3.

Euphotic zone

residual Ekman pumping

eddy exchange

horizontal mixing

biological pump

vertical mixing

residual Ekman transport

Mode water

horizontal mixing

biological pump

vertical mixing

residual Ekman transport

Abyss

0
−50
−100
−150
−200
−250
−300
−350
−400

0
250
500
750
1000
1250
1500
1750
2000

Depth (m)

Distance from gyre centre (km)

Figure 4.

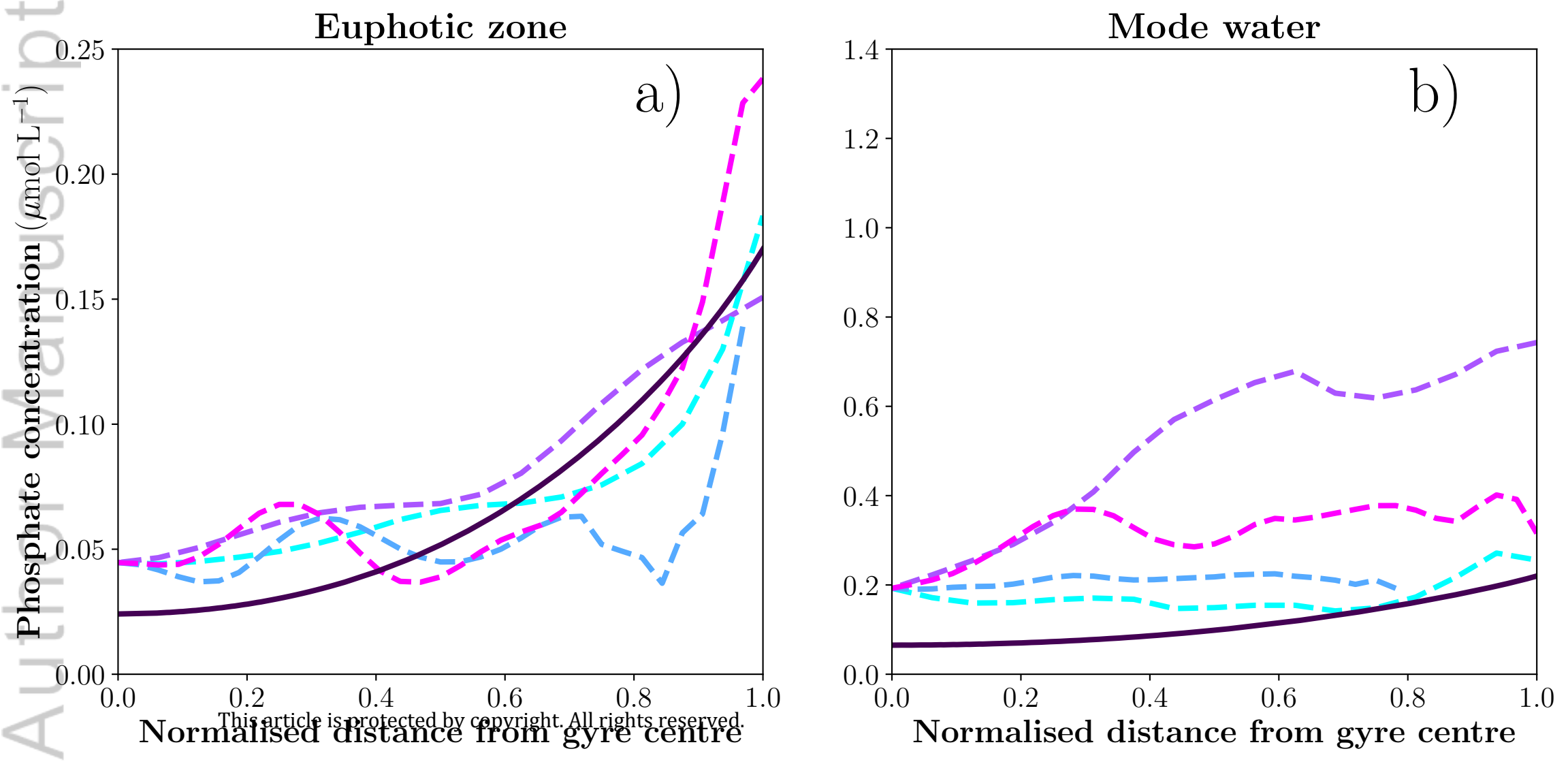

Figure 5.

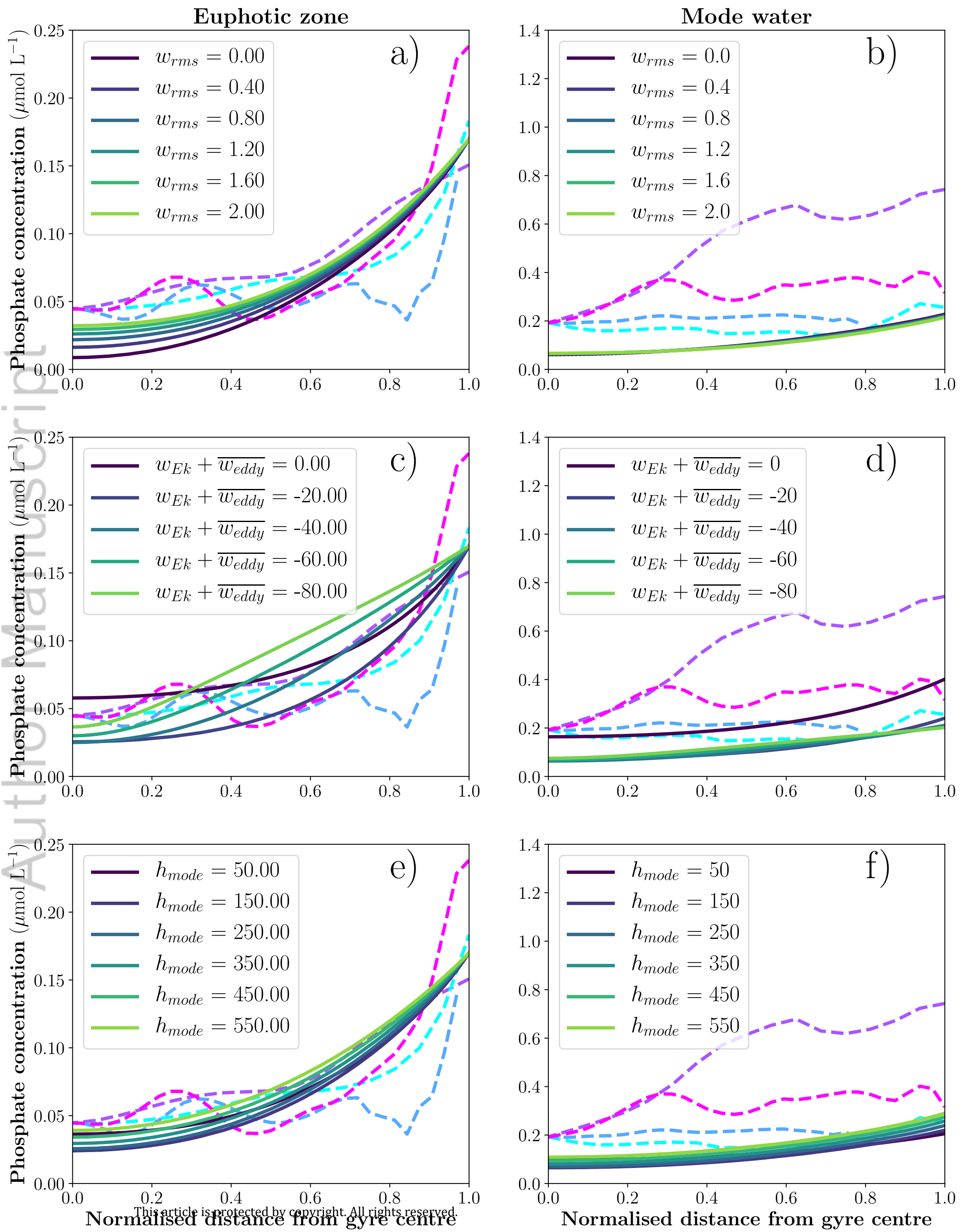

Figure 6.

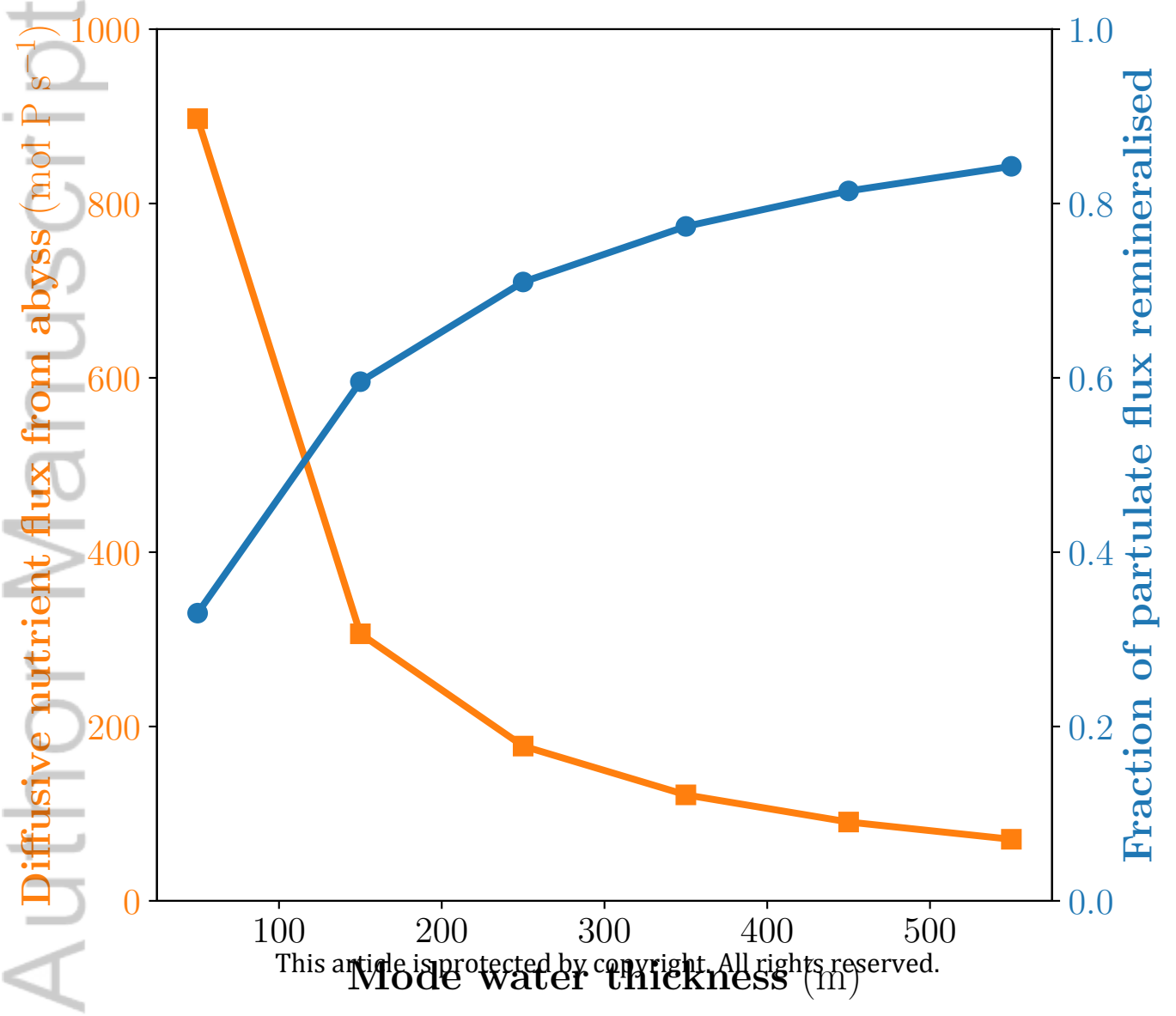

Figure 7.

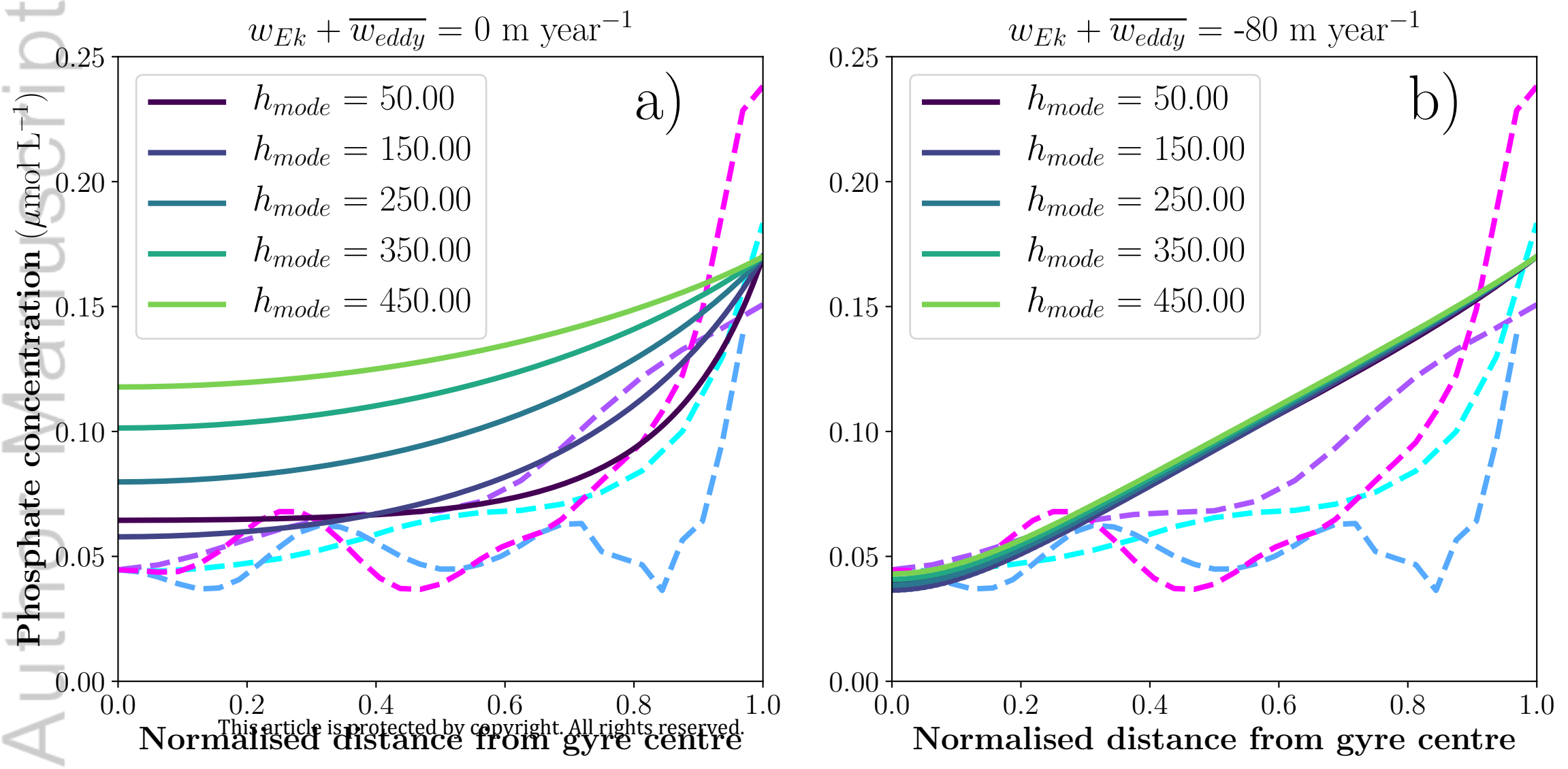

Figure 8.

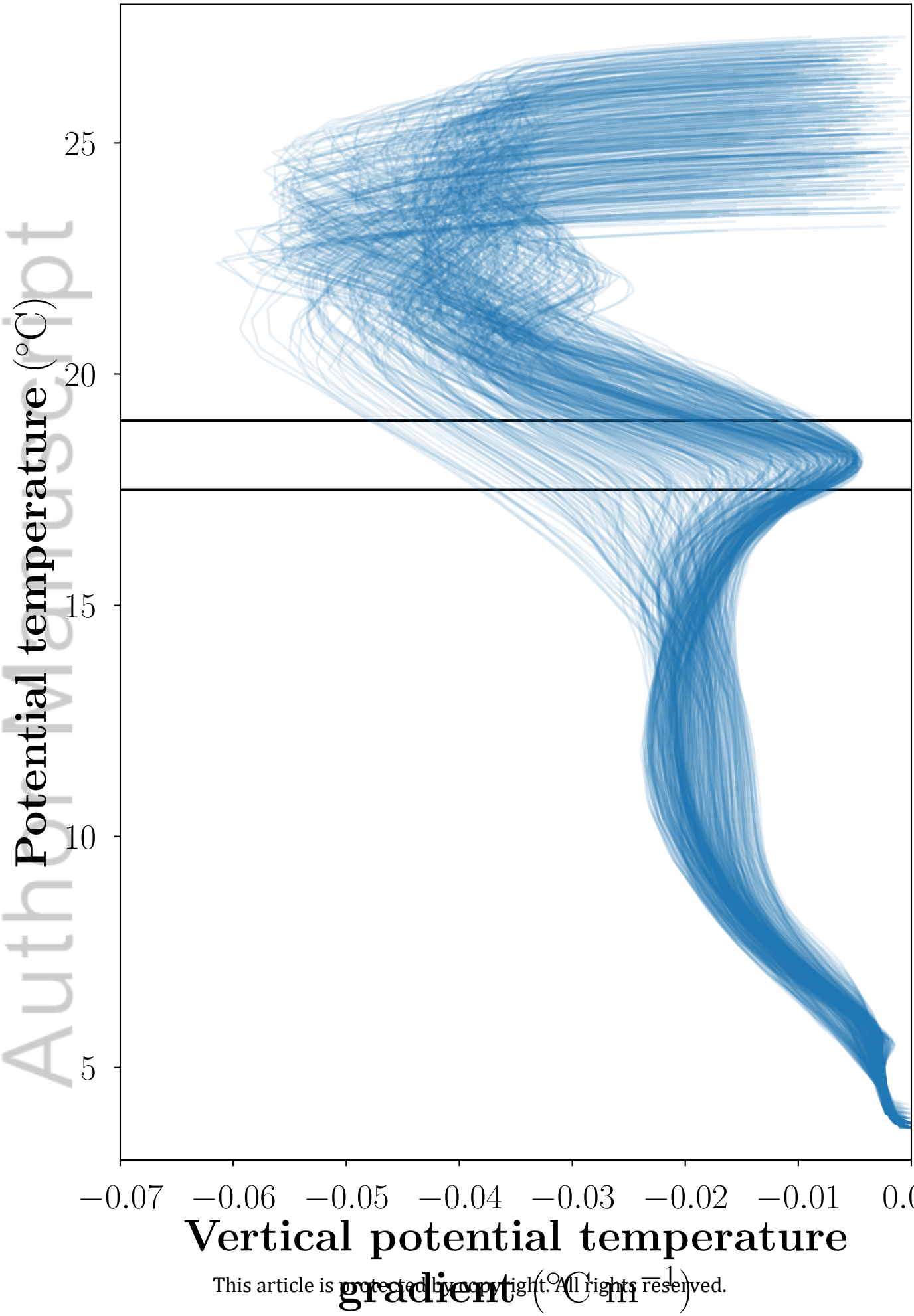

Figure 9.

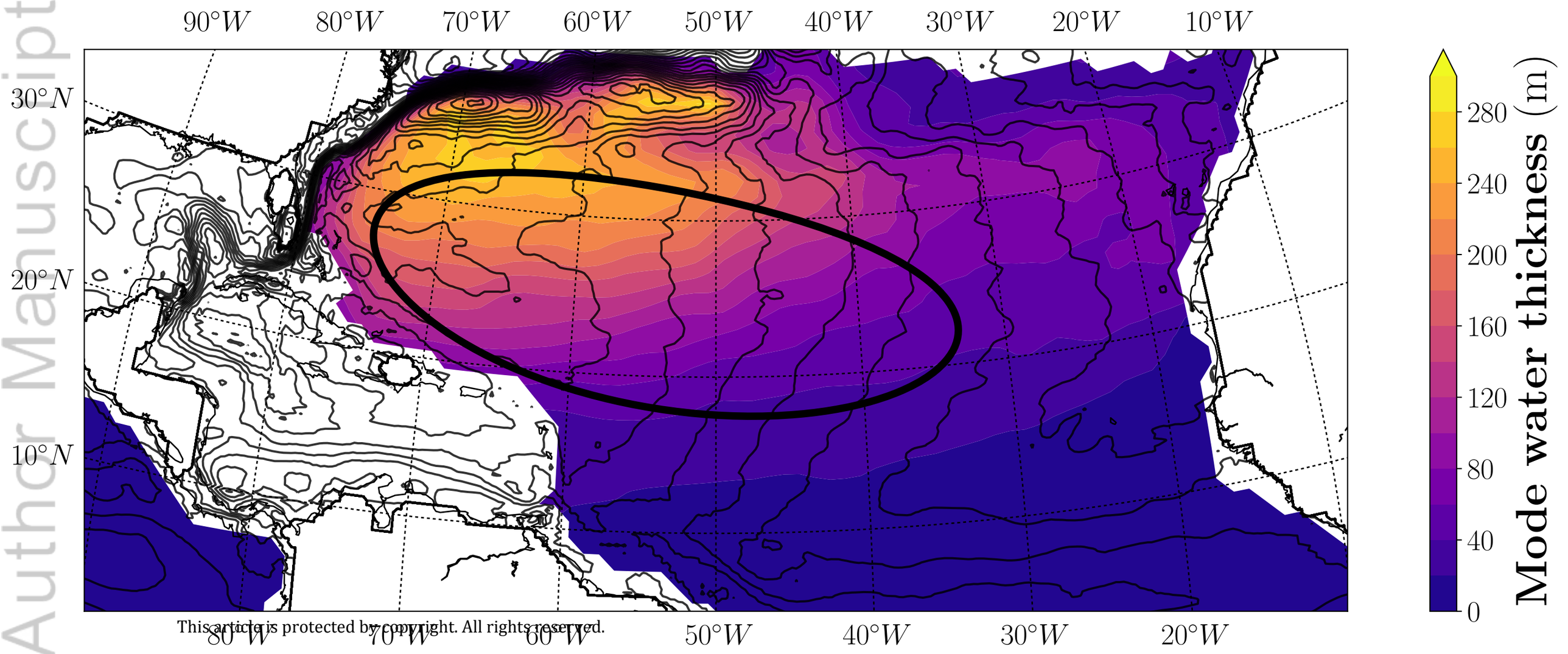

Figure 10.

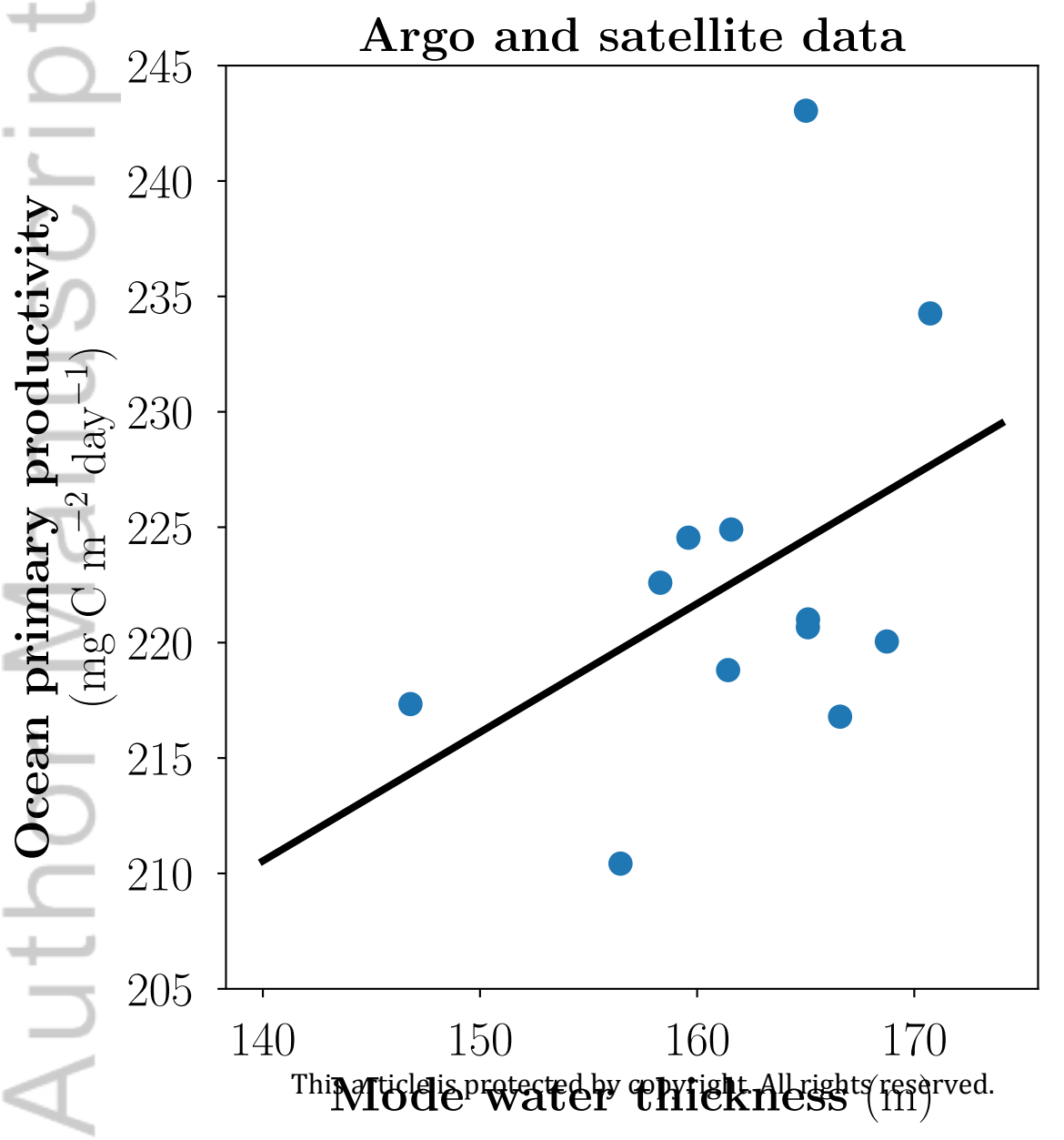

Figure 11.

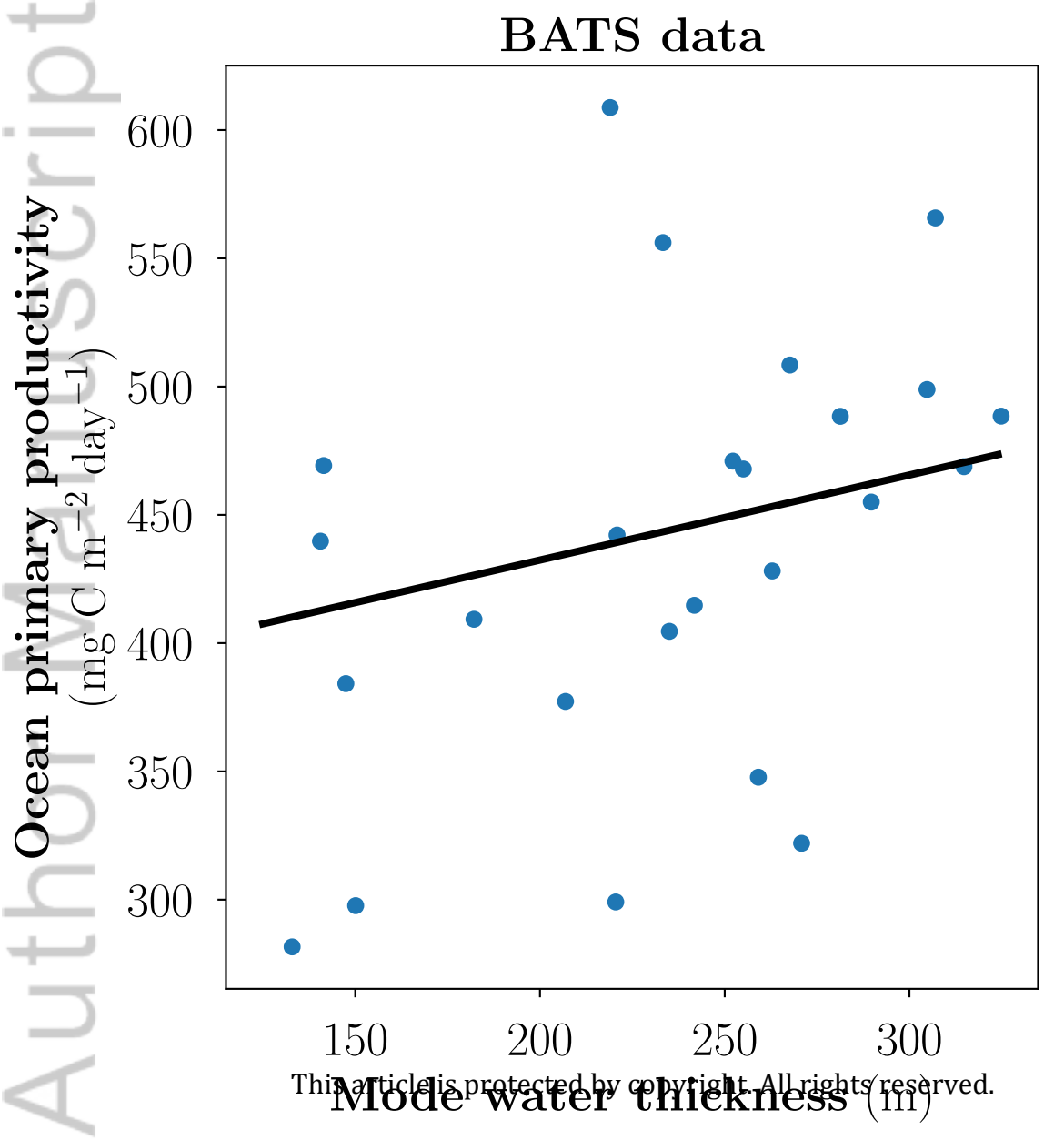

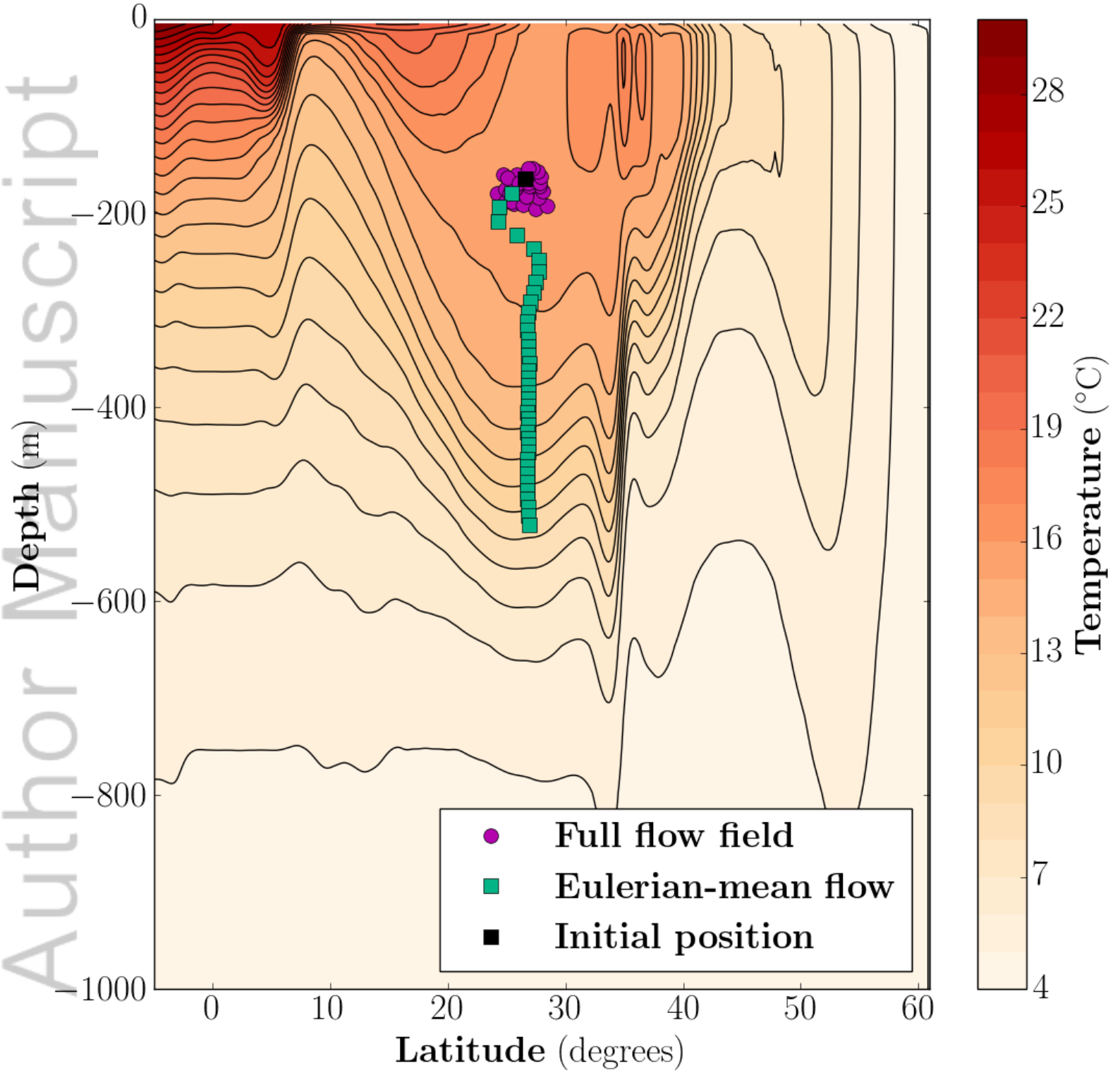

2018JC013842-f01-z-.png

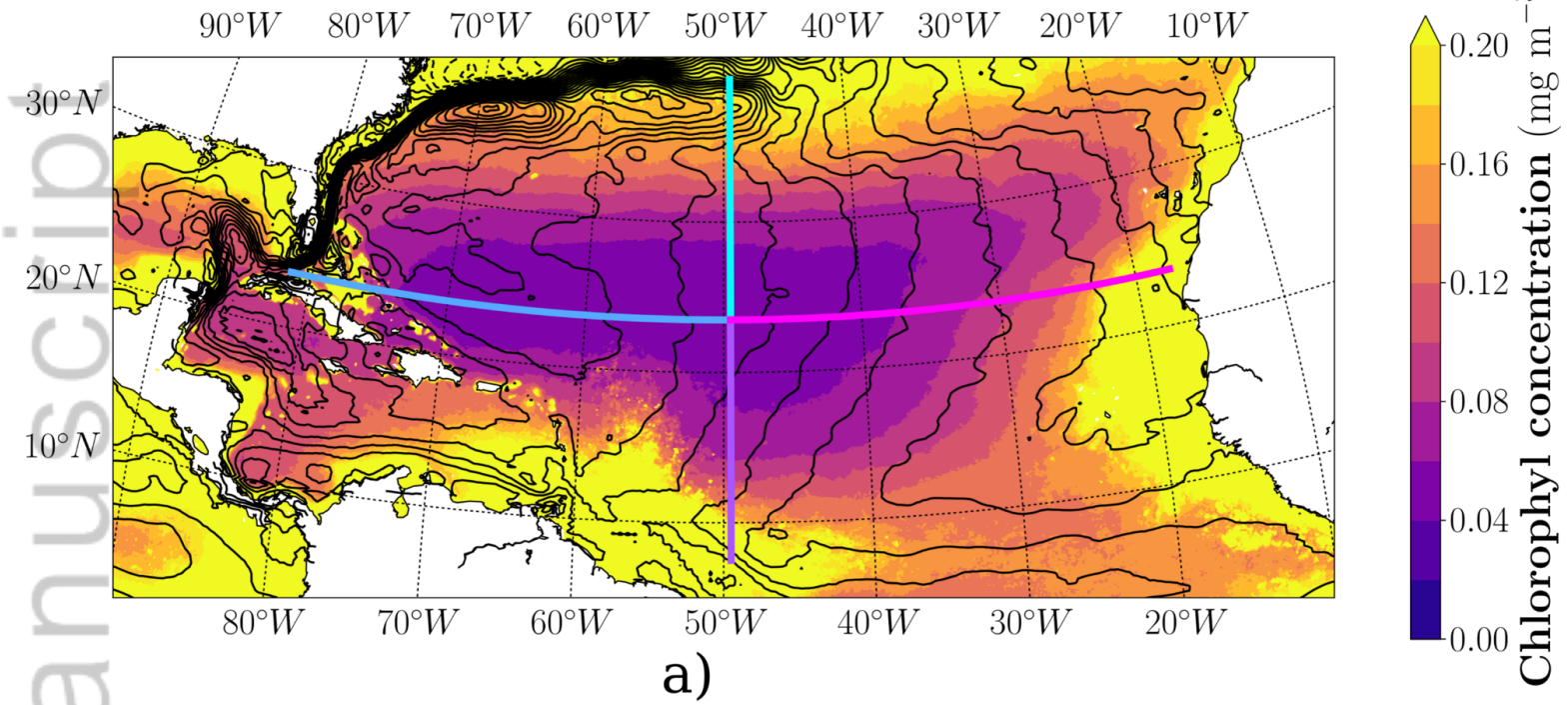

a)

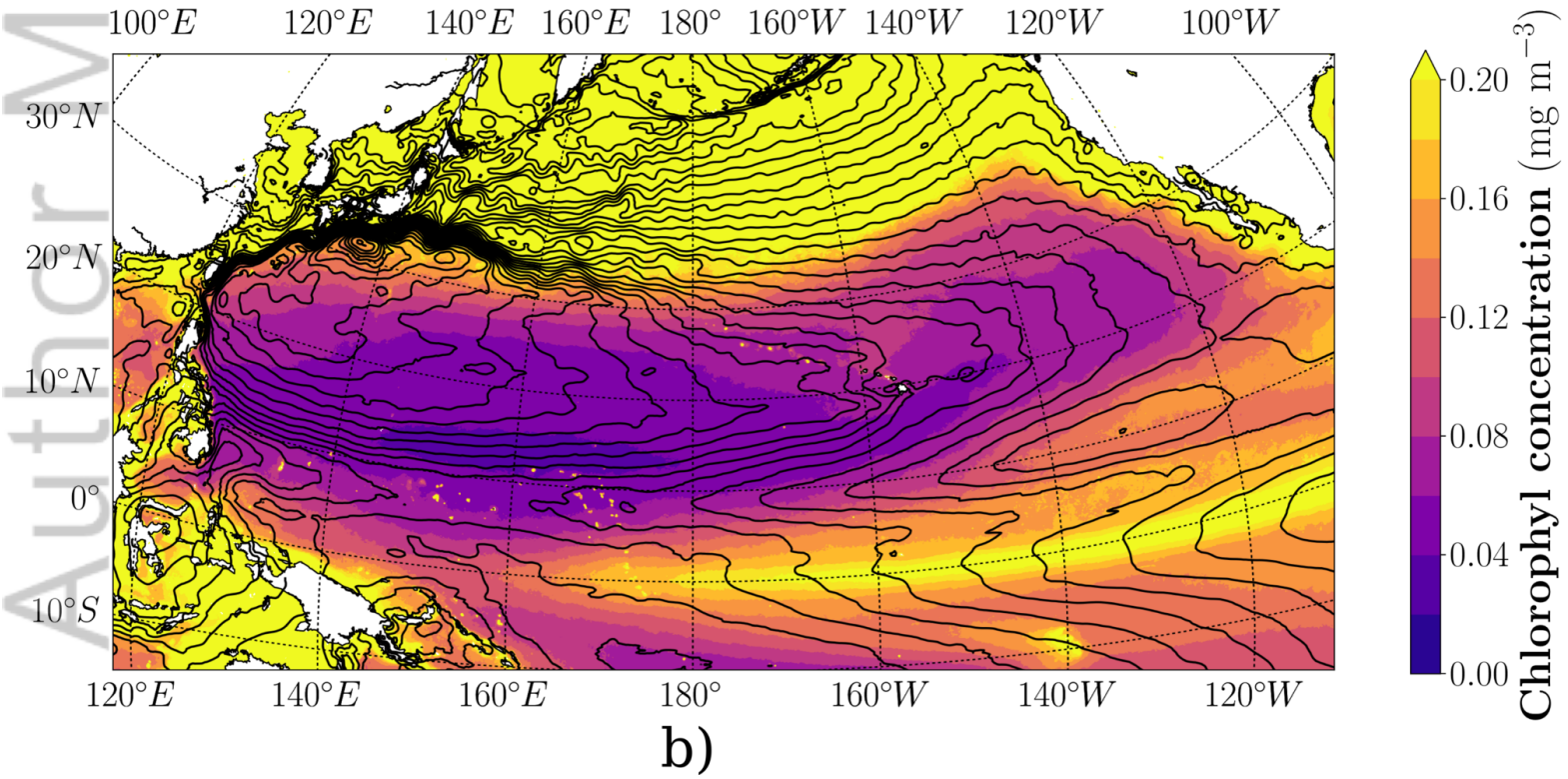

b)

2018JC013842-f02-z-.png

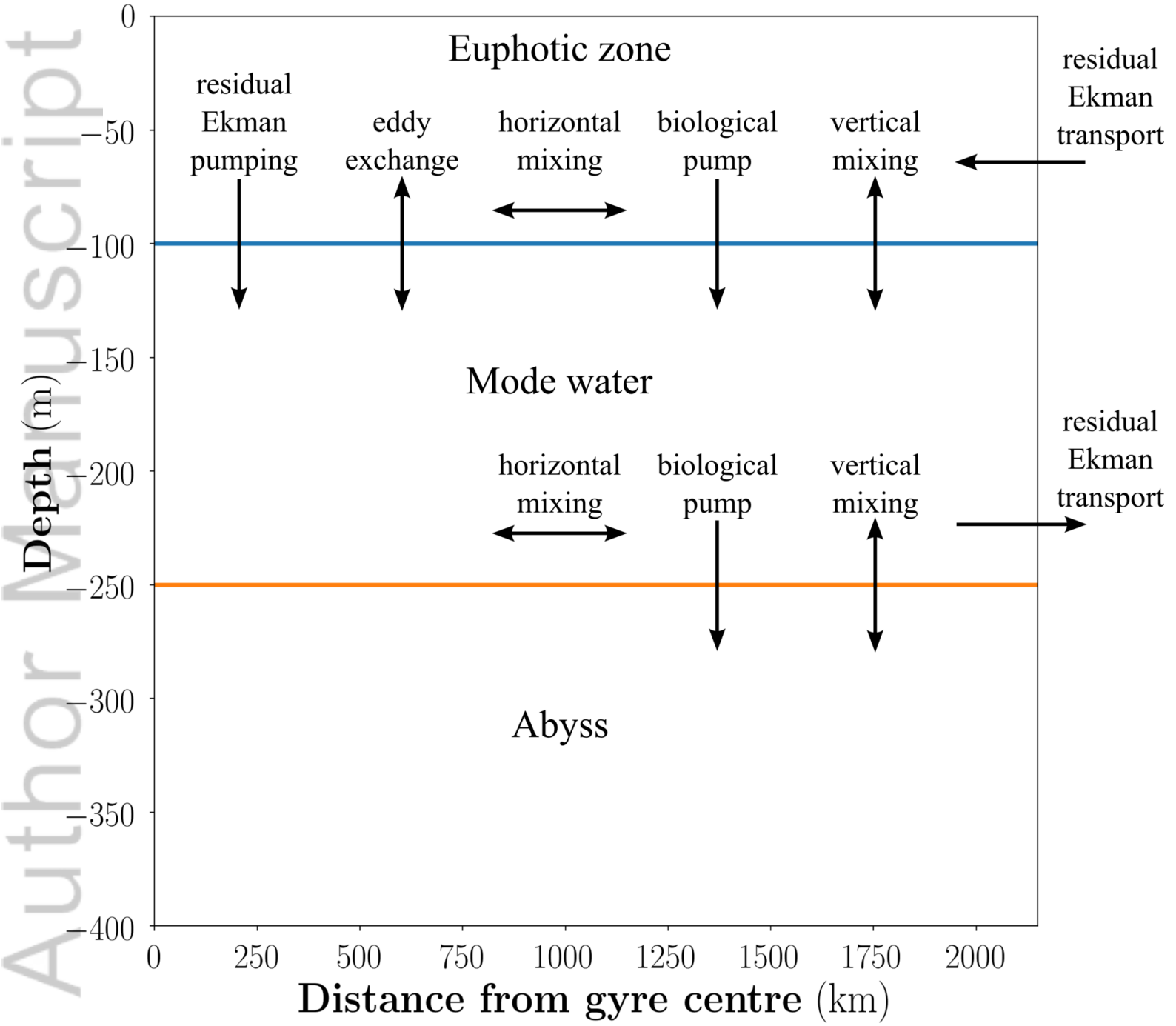

2018JC013842-f03-z-.png